Biochemical and Structural Characterization of *Cryptosporidium parvum* Lactate Dehydrogenase

William J. Cook[a*], Olga Senkovich[b*], Agustin Hernandez[c], Haley Speed[b], Debasish Chattopadhyay[b,d †]

[a]Department of Pathology, [b]Center for Biophysical Sciences and Engineering, University of Alabama at Birmingham, Birmingham, AL 35294

[c]Instituto de Bioquímica Vegetal y Fotosintesis (CSIC/U. Sevilla), Avda. Americo Vespucio 49, Seville 41092, Spain

Department of Medicine, University of Alabama at Birmingham, Birmingham, AL 35294

[†] Corresponding author: debasish@ uab.edu

Phone: (205) 934-0124

Fax: (205) 934-0480

*These authors contributed equally

Keywords: Crystal structure, lactate dehydrogenase, *Cryptosporidium parvum*

Abstract

The protozoan parasite *Cryptosporidium parvum* causes waterborne diseases worldwide. There is no effective therapy for *C. parvum* infection. The parasite depends mainly on glycolysis for energy production. Lactate dehydrogenase is a major regulator of glycolysis. This paper describes the biochemical characterization of *C. parvum* lactate dehydrogenase and high resolution crystal structures of the apo-enzyme and four ternary complexes. The ternary complexes capture the enzyme bound to NAD/NADH or its 3-acetylpyridine analog in the cofactor binding pocket, while the substrate binding site is occupied by one of the following ligands: lactate, pyruvate or oxamate. The results reveal distinctive features of the parasitic enzyme. For example, *C. parvum* lactate dehydrogenase prefers the acetylpyridine analog of NADH as a cofactor. Moreover, it is slightly less sensitive to gossypol inhibition compared with mammalian lactate dehydrogenases and not inhibited by excess pyruvate. The active site loop and the antigenic loop in *C. parvum* lactate dehydrogenase are considerably different from those in the human counterpart. Structural features and enzymatic properties of *C. parvum* lactate dehydrogenase are similar to enzymes from related parasites. Structural comparison with malate dehydrogenase supports a common ancestry for the two genes.

1. Introduction

The apicomplexan parasite *Cryptosporidium parvum* causes waterborne diseases and poses a threat to water supplies worldwide (Leitch & He, 2012; Shirley *et al*., 2012). The parasite infects a wide spectrum of hosts including humans and other mammals (Santin, 2013). In developing countries, Cryptosporidium is a significant cause of diarrhea, contributing to malnutrition in children. Although infection causes self-limited diarrhea in healthy adults, symptoms can be serious, long lasting, and often lethal in immunocompromised individuals (Leitch & He, 2012; Shirley *et al*., 2012). Currently, there is no satisfactory chemotherapy or vaccine against cryptosporidiosis.

One of the major impediments to identifying therapeutic targets in Cryptosporidium is the lack of knowledge about its biochemical and metabolic pathways. Genome sequencing indicates that *C. parvum* does not have a functional mitochondrion and lacks an active Krebs' cycle (Abrahamsen *et al*., 2004) but encodes all glycolytic enzymes. Since the parasite appears to depend primarily on anaerobic oxidation of glucose for energy metabolism (Coombs, 1999, Denton *et al*., 1996), enzymes in the glycolytic pathway and those that play

regulatory roles may offer potential targets for anti-cryptosporiodial drugs. Studies with other apicomplexan parasites have shown that inhibition of glycolysis may be a useful strategy for antiparasitic therapy (Basco *et al*., 1995; Bressi *et al*., 2000; Dando *et al*., 2001; Deck *et al*., 1998; Wang, 1984). To develop a detailed understanding of the key regulatory mechanisms that are characteristic of the parasite, we are studying a number of enzymes that control glycolysis in *C. parvum* (Senkovich *et al*, 2005; Cook *et al*., 2009; Cook *et al*., 2012).

Lactate dehydrogenase (LDH) plays a central role in regulating glycolysis. LDH is a key enzyme for the anaerobic respiration step in which pyruvate is reduced to lactate with the concomitant oxidation of NADH to NAD^+ (Everse & Kaplan, 1973). This reaction is crucial for progression of glycolysis. Firstly, removal of pyruvate allows glycolysis to progress in the direction toward generating more ATP molecules. Secondly, it regenerates NAD^+, which is required for the oxidation of glyceraldehyde 3-phosphate in glycolysis, a step catalyzed by the glycolytic enzyme glyceraldehyde 3-phosphate dehydrogenase.

In humans there are two major forms of LDH. The M-form is found predominantly in anaerobic tissues such as skeletal muscle, and the H-form is present mostly in aerobic tissues such as cardiac muscle. The M-form and H-form enzymes are 78% identical in their primary sequences. Although the primary sequence of LDH is highly conserved among various organisms, LDHs of a number of protozoan parasites including *C. parvum* (CpLDH) differ from human LDH in several key amino acid positions, and some possess a unique insertion in the active site loop (Fig. 1) (Deck *et al*., 1998; Gomez *et al*., 1997; Dunn *et al*., 1996; Sessions *et al*., 1997; Winter *et al*., 2003). LDHs of certain protozoa also demonstrate distinctive structural and biochemical properties. For example, the *P. falciparum* enzyme (PfLDH) exhibits 200-300 fold higher activity with the NADH analog 3-acetyl pyridine adenine dinucleotide (APADH) than the human M and H isozymes (Gomez *et al*., 1997). Biochemical differences between human LDH and PfLDH have been exploited for the development of a diagnostic tool for detection of malaria in the blood of infected individuals (Klenerman & Dickson, 1992; Makler & Hinrichs, 1993) and development of selective inhibitors of the parasitic enzyme (Gomez *et al*., 1997). Differences in the cofactor binding sites of LDH from human and *P. falciparum* allow derivatives of the natural product gossypol to selectively inhibit parasitic LDHs (Dando *et al*., 2001; Deck *et al*., 1998; Royer *et al*., 1998). Structural analysis of LDH from two different species of plasmodium showed that these enzymes possessed distinctive features, which may be useful for development of

species-specific inhibitors of the plasmodium enzymes (Dunn *et al*., 1996; Sessions *et al*., 1997; Winter *et al*., 2003).

Here we describe the results of enzymatic and structural analyses of CpLDH. We discuss the crystal structures of the apo-enzyme and four ternary complexes with substrate, inhibitor (oxamate) or product bound at the active site. To visualize the differences in the binding of NAD and APAD at the cofactor binding pocket, structures of pyruvate complexes were determined separately with each cofactor. We also compare the properties of CpLDH with LDHs from human and apicomplexan parasites. Finally, we present a comparison of the structures of CpLDH and *C. parvum* malate dehydrogenase (CpMDH).

2. Materials and Methods

2.1. Preparation of enzyme

Expression and purification of CpLDH have been described in detail (Senkovich *et al*., 2005). Briefly, the recombinant protein was expressed in *E. coli strain* Rosetta (DE3)pLysS. The bacterial cell pellet was lysed in buffer I (50 mM Tris-HCl, 1 mM benzamidine hydrochloride, 0.1 mM PMSF, 5 mM DTT and 1 mM EDTA, pH 7.4). The resulting suspension was subjected to centrifugation at 20,000 rpm for 30 min, and the supernatant was treated with 0.2% protamine sulfate for 20 min at 4°C. CpLDH was precipitated from clarified cell-free extract by adding ammonium sulfate to 40% saturation. The resuspended pellet was dialyzed overnight in buffer I and applied to a Superdex 200 size exclusion column (Amersham Pharmacia). As reported previously, enzymatically active CpLDH eluted from the Superdex 200 column as a tetramer as calculated from the elution volume and = nearly homogeneous purified protein migrated as a major band of approximately 33 kDa on SDS-PAGE (Senkovich *et al*., 2005). Fractions containing enzymatically active CpLDH were pooled, dialyzed against buffer II (50 mM Tris-HCl, 1 mM EDTA and 5 mM DTT, pH 8.0) and applied to a Mono Q 10/10 column (Amersham Pharmacia). After washing the column with buffer II, the bound protein was eluted using a linear gradient of sodium chloride (0-0.3 M) in 15 column volumes of buffer II. Purified protein was concentrated by ultrafiltration to a final concentration of 21 mg/ml. Sequencing of the recombinant plasmid revealed that the DNA encodes alanine at position 202, lysine at position 265 and glutamate at position 311 (see Footnote for explanation of LDH numbering), while the database sequence for CpLDH (GenBank accession No. AF274310) has valine, arginine and lysine, respectively, at these positions (Fig. 1). Similar results were obtained in multiple PCR experiments. We do not

know if the sequence differences are PCR errors, mutations corresponding to DNA polymorphism, or if there are errors in the GenBank database.

2.2. Enzyme activity

LDH enzyme assays were performed in a temperature-controlled UV-Visible spectrophotometer (DU740, Beckman Instruments) using standard methods (Dando *et al*., 2001). Reaction velocities were measured at 25°C for 1 min by following decrease or increase in absorbance at 340 nm due to oxidation of NADH or reduction of NAD^+. The CpLDH activity in the direction of reduction of pyruvate to lactate was measured in 50 mM sodium acetate buffer, pH 5.5, and activity in the direction of oxidation of lactate to pyruvate was measured in 50 mM Tris-HCl buffer, pH 9.1. A typical reaction mixture contained substrate (10 μM - 5 mM pyruvate or 50 μM - 20 mM lactate) and cofactor (3 - 150 μM NADH or 10 - 600 μM NAD^+); enzyme reaction was initiated by adding 1 - 5 μg of purified CpLDH. The pH dependence of the CpLDH activity was determined using three buffers with overlapping pHs: 50 mM sodium acetate, pH 3.6 - 6.0, 50 mM sodium phosphate, pH 5.6 - 7.2 and 50 mM Tris-HCl, pH 6.6 - 9.5. When $APAD^+$/APADH was used as cofactor, reaction velocities were measured by following increase or decrease in absorbance at 363 nm due to reduction of $APAD^+$ or oxidation of APADH. The kinetic parameters (Michaelis constant K_m, maximum velocity V_{max} and turnover rate K_{cat}) for substrates and cofactors and the inhibitory constant K_i value for gossypol were determined by non-linear regression using ANEMONA Excel templates (Hernandez and Ruiz, 1998).

2.3. Crystallization and data collection

CpLDH was crystallized under several different conditions at 4°C. As reported previously crystals of the apo enzyme suitable for data collection were grown from 16.5% (v/v) PEG 2000, 0.1 M Tris-HCl (pH 7.0) and 0.08% n-octyl-β-D-glucopyranoside (Senkovich *et al*., 2005). For crystallization of the ternary complexes, the concentrated protein was incubated with 1 mM substrate (pyruvate, lactate or oxamate) and 100 μM NADH, NAD^+ or $APAD^+$ for an hour on ice. Crystals of the ternary complexes were obtained at 4°C using 1.45-1.65 M ammonium sulfate in 0.1 M sodium cacodylate (pH 6.75 to 7.25).

X-ray diffraction data were collected under cryogenic conditions (-180°C) using a cryopreservative solution containing 25% glycerol in the reservoir solution. Intensity data were processed using Denzo and Scalepack (Otwinowski & Minor, 1997). Crystals of apo CpLDH belong to space group $P3_212$ and contain four monomers (two dimers) in the asymmetric unit. Crystals of the ternary complexes belong to space group $P3_221$ and contain two monomers (one dimer) in the asymmetric unit.

2.4. Structure determination and refinement

The crystal structure of the ternary complex of CpLDH with pyruvate and $APAD^+$ was solved by molecular replacement using the CNS program package (Brünger *et al*., 1998) with data in the range 20 - 4.5 Å for the rotation and translation searches. Calculation of a self-rotation function revealed a strong peak at kappa = 180º, indicating the presence of a noncrystallographic two-fold axis. Using a search model of CpLDH built from PfLDH (PDBID 1T2D), positions of the two monomers in the asymmetric unit were determined.

The correct enantiomorphic space group ($P3_221$) was determined from the values of correlation coefficient and R factor in the molecular replacement trials with the two enantiomorphic space groups. Refinement of the structure was performed initially by simulated annealing using CNS with the stereochemical parameter files defined by Engh and Huber (1991). No sigma cutoff was applied to the data. Ten percent of the data was randomly selected and removed prior to refinement for analysis of the free R factor. The two subunits in the asymmetric unit were restrained by the non-crystallographic symmetry throughout the simulated annealing refinement. The molecular model was improved by cycles of manual fitting to 2Fo-Fc electron density maps using the program COOT (Emsley *et al*., 2010) alternating with refinement.

An Fo-Fc electron density map allowed placement of $APAD^+$ and pyruvate in each monomer. As the refinement progressed, water molecules were added by using the water-picking routines in CNS and COOT. All water molecules were verified by inspection of the maps. In the later stages of refinement, noncrystallographic symmetry restraints were removed, and the restrained refinement option in REFMAC5 (Murshudov *et al*., 2011) was used.

The structures of the apo enzyme and the other three ternary complexes were solved by molecular replacement using the LDH dimer from the *C. parvum* LDH/$APAD^+$/pyruvate

structure as the search model. The refinement procedure was the same in each case as described above. Atomic coordinates and structure factors have been deposited in the Protein Data Bank with PDBIDs *4ND1* (NAD^+/oxamate complex), *4ND2* ($APAD^+$/pyruvate complex), *4ND3* (NADH/lactate complex), *4ND4* (NAD^+/pyruvate) and *4ND5* (apo enzyme)[†].

3. Results

As reported previously purified recombinant CpLDH eluted as a tetramer as revealed by size exclusion chromatography (Senkovich *et al*., 2005). On SDS PAGE analysis the purified protein migrated as a single band of approximately 33 kDa.

3.1. Enzyme activity

Using buffer solutions of overlapping pH, we determined pH optima for LDH reactions in both directions. The optimal pH for the reduction of pyruvate was 5.0 - 5.5, but the optimal pH for the oxidation of lactate was 9.0 - 9.5 (Fig. 2A and B). In Table 1, kinetic parameters for CpLDH are compared with those of human isoforms, *P. falciparum* and *T. gondii* LDH. Like PfLDH, CpLDH prefers $APAD^+$ and APDH over NAD^+ and NADH, respectively, as a cofactor. The k_{cat} of CpLDH was two-fold greater for APADH than for NADH. Similarly, the enzymatic activity of CpLDH was ~5 times higher with $APAD^+$ than with NAD^+ as a cofactor. On the other hand, the human enzymes show ~17-20 fold higher activity with NAD^+ as compared with $APAD^+$. Therefore, with $APAD^+$ the activity of CpLDH is 100 fold higher than the human counterparts. In comparison PfLDH is 200 times more active with $APAD^+$ than the human enzyme (Gomez *et al*., 1997). In the case of CpLDH a small but significant negative cooperativity towards pyruvate was observed (Hill coefficient h= 0.69±0.00). However, in the case of NADH, the estimated cooperativity (Table 1) was not significant since the sum of least-squares after fitting the data to a Hill model was nearly identical to that observed after a pure Michaelis-Menten fit (data not shown). On the other hand, a negative cooperativity was observed when $APAD^+$ was used as a cofactor.

Gossypol and a number of its derivatives are known to inhibit LDH activity (Deck *et al*., 1998; Conners *et al*., 2005). As seen with other LDHs (Olgiati & Toscano, 1983), the

[†] PDBIDs are shown in italics throughout this manuscript

mechanism of inhibition of CpLDH by gossypol is competitive with NADH (Fig. 2C). The observed K_i value for gossypol (11.6 μM) for CpLDH is in the same range but slightly higher than for the human enzyme (1.9 and 1.4 μM for M and H-forms, respectively; Gomez *et al*., 1997).

In general, LDHs are inhibited by excess pyruvate, presumably due to the formation of an NAD^+/pyruvate complex (Wang, 1977). A distinctive biochemical feature of some protozoan LDHs is their insensitivity to high pyruvate concentration. As shown in Fig. 2D, CpLDH does not display any measurable inhibition to pyruvate concentrations up to at least 20 mM.

3.2. General description and quality of the structures

Crystal structures of CpLDH were determined in the apo form and as ternary complexes containing the following: pyruvate and NAD^+, lactate and NADH, oxamate and NAD^+, pyruvate and $APAD^+$. Statistics for data collection are shown in Table 2. Refinement statistics and Molprobity analyses (Davis *et al*., 2007) are listed in Table 3.

3.2.1. Apo CpLDH

Apo CpLDH crystallizes in the space group $P3_212$, and the crystal structure contains two dimers (two half tetramers) in the asymmetric unit. The crystallographic symmetry pairs for each dimer form the functional tetramers. The model includes residues 17-98 and 112-330 for monomer A, 17-98 and 112-329 for monomer B, 18-98 and 112-329 for monomer C, and 18-98 and 112-327 for monomer D. The electron density for C-terminal residues and the active site loop (residues 99-111) was extremely weak, and those residues could not be modeled. The four CpLDH monomers in the asymmetric unit are nearly superimposable. Compared to monomer A, the root mean square deviation for all Cα-atoms is 0.327 Å for B to A, 0.353 Å for C to A and 0.332 Å for D to A.

3.2.2. Ternary complexes of CpLDH

Crystals of the four ternary complexes belong to space group $P3_221$.The asymmetric unit contains two monomers related by non-crystallographic 2-fold symmetry (Fig. 3A). The complete tetramer is formed with their symmetry partners related by a crystallographic 2-fold axis. In each complex the model includes residues 17-333 for each chain (see note at the end

of the manuscript); only the last four C-terminal residues were not visible in the electron-density maps. The arrangement of the monomers in the tetramer is similar to that seen in other LDH structures. The two monomers in the asymmetric unit form the major interface and bury approximately 7900 $Å^2$ of surface area. Superposition of all four complex structures, using monomer A of the CpLDH/NAD^+/pyruvate structure as the reference, results in r.m.s.d. values of 0.113 Å for CpLDH/NADH/lactate, 0.176 Å for CpLDH/NAD^+/ oxamate, and 0.107 Å for CpLDH/$APAD^+$/pyruvate.

As shown in Supplementary Fig. S1, in all four ternary complexes the NAD^+/NADH site is fully occupied in both monomers in the asymmetric unit. Electron density for substrate molecules was also excellent in each subunit of all complexes except in the NADH/lactate complex, in which the density for lactate was clear only in subunit A. Average B-factors for the co-factor and substrate/analog molecules are comparable to those of the protein residues in each complex (Table 3). In all cases the CpLDH monomers in the asymmetric unit and the bound cofactors are nearly superimposable. The root mean square deviation between monomers A and B for all 317 Cα atoms is 0.278 Å for CpLDH/NAD^+/pyruvate, 0.465 Å for CpLDH/NADH/lactate, 0.379 Å for CpLDH/NAD^+/oxamate, and 0.347 Å for CpLDH/$APAD^+$/pyruvate.

The overall quality of the structures of CpLDH is excellent. Only Ala164 and Gly283 in each monomer exhibit phi, psi angles in non-allowed regions of the Ramachandran plot. The residue corresponding to Ala164 is glycine in human and plasmodium LDH. All of the structures contain several glycerol molecules associated with each chain.

3.3. NADH/APADH and substrate binding sites

In the following description monomer A from the ternary complex CpLDH/NAD^+/pyruvate (*4ND4*) will be used as the template unless otherwise stated. CpLDH monomers are composed of two domains with the active site located at the interface of the two domains (Fig. 3A). The NAD-binding domain (shown in light pink in Fig. 3A) is characterized by a typical Rossmann fold consisting of a six-stranded parallel β-sheet flanked by α-helices. As shown in Fig. 3B and C, the adenine ring of the cofactor lies in a hydrophobic pocket formed by Ile27, Phe52, Ile54, Tyr85, Ala98, Ile119 and Val123 and packs against the side chains of Ile54 and Ala98. The hydroxyl oxygen atoms O2B and O3B

of the adenosine ribose ring are hydrogen bonded to the side chain oxygen atoms of Asp53. The diphosphate oxygen atoms are hydrogen bonded to water molecules and main chain N atoms of Gln31 and Ile32. The nicotinamide ring packs against the hydrophobic side chains of Ile32, Ile138 and Pro250 (Fig. 3B). The hydroxyl oxygen atoms O2D and O3D of the nicotinamide-ribose are hydrogen bonded to the ND2 atom of Asn140 and the OG atom of Ser99, respectively (Fig. 3D).

The conserved catalytic residues Arg171 and His195 (CpLDH numbering), which bind the substrate, are located in the catalytic domain (shown in magenta in Fig.3A). The carboxyl oxygen atoms (O1 and O2) of pyruvate form hydrogen bonds with the side chain nitrogen atoms of Arg171, and O2 forms an additional contact with NH2 of Arg109. Atom O3 of pyruvate forms hydrogen bonds with atom NE2 of His195 and atom NE of Arg109 (Fig. 3D).

3.4. Changes to apo-LDH on binding of substrate and cofactor

As expected, the overall structure of CpLDH is similar in the apo-form and various ternary complexes. Compared to monomer A in the CpLDH/NAD^+/pyruvate structure, the r.m.s.d. deviation for all Cα-atoms is 0.883 Å. The major differences between the apo and complex structures are confined to five regions, and four of these regions are involved in binding the cofactor and the substrate. The most obvious difference is the absence of electron density for the active site loop (residues 99-111, Fig. 4A), indicating disorder in the apo structure. The second region, residues 138-145, corresponds to the end of a short loop and the beginning of helix 4 (Fig. 4B). This segment moves closer to the active site loop when the active site is occupied. The third region, residues 194-198, includes the conserved catalytic residue His195. The side chain of His195 assumes a different rotamer configuration in the apo structure (Fig. 4C). This is different from the plasmodium and toxoplasma apo LDH structures, in which the side chain of the catalytic histidine residue has the same rotamer conformation as in substrate-bound LDH. The fourth region (residues 234-245) is at the end of a long helix (Fig. 4D). This helix moves closer to the substrate in the CpLDH/NAD^+/pyruvate structure. Finally, the long C-terminal helix moves closer to the adjacent beta sheet to form a slightly more compact structure overall (Fig. 4A), but it does not seem to have any effect on the binding site.

4. Discussion

4.1. Comparison to human LDH

The crystal structures of human LDH have been determined in the apo form, as a binary complex with NADH (Dempster *et al*., 2014) and as ternary complexes (Read *et al*., 2001). The sequence identity between CpLDH and human LDH is 25%, and the r.m.s.d. value for the superposition of CpLDH (NAD^+/oxamate complex) with the H form of human LDH bound to NADH and oxamate (PDBID: 1I0Z) is 1.050 Å. The overall architecture of CpLDH is similar to the structure of human LDH, and most of the structural differences are small and involve peripheral loops and the C-terminus (Fig. 5A). However, there are two major differences. Conformation of the active site loop in CpLDH (residues 99-111) is considerably different from human LDH, even though it contains the same number of residues in both enzymes. Moreover, the helix-loop segment (residues 243-245) in the CpLDH structure also moves closer to the active site loop. A close-up view of the two above mentioned loops in the two structures is displayed in Fig. 5B. Electron density for the CpLDH residues in both loops was well defined (see Supplementary Fig. S2). The other major conformational difference between these structures is in the antigenic loop (CpLDH residues 210-225, Fig. 5C, also Supplementary Figure S3). This loop has a similar conformation in the cryptosporidium, plasmodium and toxoplasma LDH structures, but in the human LDH structure the loop pivots on residues Leu211 and Trp227 (corresponding to Leu212 and Ile225 in CpLDH) away from the N-terminus of the adjacent monomer in the tetramer. The N-terminal extension in human LDH structures is not present in cryptosporidium, plasmodium or toxoplasma LDH and probably explains the large conformational change of the antigenic loop with respect to parasitic LDH. The four critical residues involved in binding the substrate (Arg109, Asn140, Arg171 and His195) are conserved in human and CpLDH. However, there are significant differences in the cofactor binding site that explain the lower affinity for NAD^+/NADH in the parasitic enzyme (discussed in section 4.4).

4.2. Comparison to Plasmodium and Toxoplasma LDH

The crystal structures of LDH from *T. gondii* (TgLDH; Kavanagh *et al*., 2004) and three species of the malaria parasite have been determined: *P. falciparum* ((Dunn *et al*., 1996), *P. vivax* (Chaikuad *et al*., 2005) and *P. berghei* (Winter *et al*., 2003). LDH structures from the three plasmodium species are almost identical, so only the *P. falciparum* LDH structure (PfLDH) will be used for comparison.

Results of primary sequence alignment using the CLUSTAL Omega server (http://www.ebi.ac.uk) (Goujon *et al*., 2010; Sievers *et al*., 2011) show that identity between

LDHs from various species varies roughly in the range 41-49% based on the evolutionary relationship between the organisms. Thus, pair-wise sequence identities between CpLDH and LDH from *P. falciparum* and *T. gondii* are 41% and 41%, respectively, while the *P. falciparum* and *T. gondii* sequences are 49% identical. The r.m.s.d. values for the superposition of CpLDH (NAD^+/oxamate complex) with TgLDH (PDBID: 1PZF) and PfLDH (PDBID: 1T2D) are 0.956 Å and 1.066 Å, respectively. Although the overall architecture of CpLDH is similar to the other two parasitic LDH structures, the orientation of the active site loop in CpLDH is quite different, primarily because this loop contains five fewer residues in CpLDH (Figs. 1 and 6A,B). The extra residues in the plasmodium and toxoplasma LDH structures cause the loop to protrude from the active site, while the absence of these extra residues in CpLDH results in a loop in which three residues (Ile100, Pro101 and Gly102) bulge out to form the surface of the binding site cavity (Fig. 6B). The conformation of the other loop that covers the active site cleft (residues 243-246; Fig. 6B) is somewhat different than in plasmodium LDH. This loop is closer to the helix (residues 222-243) o the other side of the binding cleft compared to the PfLDH structure, which has a two residue deletion in the helix. The remaining structural differences are small and involve peripheral loops and the C-terminus. The antigenic loop of CpLDH (residues 210-225) is similar to that in the PfLDH and TgLDH structures.

The four residues involved in binding the substrate and co-factor are conserved in all three parasitic enzymes. In PfLDH a leucine residue is present in the position equivalent to Met163 in CpLDH, while in TgLDH the equivalent residue is also methionine. Both PfLDH and TgLDH contain a proline residue in the position equivalent to Pro250 in CpLDH.

Gossypol and a number of its derivatives have been reported to inhibit PfLDH at low micromolar or nanomolar concentration ranges. So far structure any LDH- gossypol complex has not been determined. Crystal structures of PfLDH with small gossypol-like compounds have been reported (*1U4O, 1U4S, 1U5C, 1U5A*). These naphthalene derivatives are much weaker inhibitors of PfLDH (than gossypol) with IC_{50} values in the millimolar range (Ki's not known). The co-crystal structures revealed two binding modes for these compounds, one overlapping the pyruvate binding site and the other bridging the binding sites for the nicotinamide ring and pyruvate (Conners *et al*., 2005). PfLDH residues (Arg171, His195) that provide the major interactions with these inhibitors are identical in CpLDH. The other interacting residue, Pro246, is replaced by an alanine in CpLDH but in this case the main

chain oxygen atom is involved in the interaction. Since these compounds are much smaller than gossypol additional protein-ligand interactions involving the remainder of gossypol structure are not known. However, these observations emphasize that in spite of the sequence similarity in the active site, subtle structural or conformational differences at or near the binding sites result in some degree of selectivity for a particular ligand.

4.3. Comparison to Malate Dehydrogenase (MDH)

LDH and MDH are homologous enzymes with a common protein fold and catalytic mechanism. Recently, evolutionary relationships among various clades of LDH/MDHs have been analyzed and discussed in detail (Boucher *et al*., 2014. In Apicomplexa, evolution of the *ldh* gene resulted from a small number of mutations of a duplicated ancestral *mdh* gene (Zhu & Keithly, 2002; Boucher *et al*., 2014). In these organisms LDH evolved independently twice, resulting in two lineages in Plasmodium-related species and in Cryptosporidium. In modern apicomplexan, LDH and MDH exhibit exquisite substrate specificity. The active site loop in these enzymes is highly significant not only in determining the rate of catalysis but also for substrate specificity (Bzik *et al*., 1993; Dunn *et al*., 1996; Waldman *et al*., 1988; Wilks *et al*., 1988). In canonical LDHs residue 102 is glutamine, while the corresponding residue in all MDHs is arginine. A single mutation of this glutamine in canonical LDHs to arginine is sufficient to alter substrate specificity by three orders of magnitude (Wilks *et al*., 1988). Thus residue 102 is termed the 'specificity residue.' Notably, the corresponding residue in apicomplexan LDH is Lys, and in the crystal structures of these LDHs this residue remains excluded from the active site. However, the most striking difference in the structures of these proteins is an insertion in the active site loop in LDH (Figure 7B). This insertion results in an alteration of the 'specificity residue' to Trp107 in modern apicomplexan LDHs (Trp107 in TgLDH, *1PZF* and Trp 94 in in PfLDH, *1T2D*). Mutation of this tryptophan residue to alanine in PfLDH results in a reduction of activity with pyruvate by five orders of magnitude (Boucher *et al*., 2014).

The r.m.s.d. value for the superposition of CpLDH (NAD^+/pyruvate complex) with CpMDH (PDBID: 2HJR) is 1.038 Å. The overall architecture of CpLDH is almost identical to that of CpMDH; the only significant difference occurs at the active site loop. The CpLDH residues involved in substrate binding are conserved in CpMDH (Fig. 7A). Boucher *et al*. (2014) suggested that Cryptosporidium LDHs are exceptional as they are clustered within the apicomplexan MDH clade separated from all other apicomplexan LDHs. Thus, residue 102,

which is lysine in all apicomplexan LDHs, is replaced by a glycine residue in CpLDH, and the five residue insertion seen in other apicomplexan LDHs is absent in CpLDH (Fig. 7B).

4.4. $APAD^+$ versus NAD^+ binding

Structural details of the cofactor binding sites in apicomplexan LDHs provide insights for understanding the basis of their preference for $APAD^+$ over the natural substrate NAD^+. In mammalian LDHs, NAD^+ binding is favored by a hydrogen-bonding network formed by a serine residue (Ser161 in human), a highly conserved water molecule and the carboxyamide group (Fig. 8A). When $APAD^+$ is substituted for NAD^+, there is a loss of these two hydrogen bonds, resulting in a lower affinity for $APAD^+$. However, in parasitic LDH structures only two hydrogen bonds are formed with NAD^+ (Fig. 8B), resulting in a lower affinity for this cofactor than the human enzyme . Furthermore, replacement of the conserved serine residue by Met163 in CpLDH (leucine in plasmodium or methionine in toxoplasma) allows a better packing environment for the acetyl group of $APAD^+$. Finally, there is a small rotation of the pyridine ring around the glycosidic bond connecting N1 and C1, which moves the methyl group away from the carbonyl oxygen atoms of Ile138 and Met163 (Fig. 9). For the LDH/$APAD^+$/pyruvate structure this torsion angle is 132.2˚, while it ranges from 144.8˚ to 146.0˚ for the three complexes that bind NAD^+/NADH. Although all of these changes are relatively small, together they are probably sufficient to explain the higher activity that PfLDH and CpLDH show with $APAD^+$ compared to human LDH. As in the case of plasmodium, the elevated activity of CpLDH with $APAD^+$ may be useful as a diagnostic tool for detection of cryptosporidium.

5. Conclusions

Although the core of the CpLDH structure is similar to human LDH, it deviates in areas of functional significance. The differences in enzymatic characteristics of CpLDH and human LDH isoforms are explained by the differences in the amino acid sequences and three-dimensional structures of these proteins. Many of the distinctive features of plasmodium and toxoplasma LDH are also conserved in the cryptosporidium enzyme. This suggests that active site inhibitors developed against enzymes of one parasite may be useful for designing broad-spectrum anti-parasitic agents.

Note

To preserve active-site nomenclature, LDHs are commonly numbered according to the initial assignment of residues from the X-ray structure of dogfish muscle LDH (Eventoff *et al*., 1977). Since the primary sequence was not available at that time, errors were made that consequently required the elimination of some numbers and the insertion of others. Insertions relative to this reference have a letter appended to the residue number (i.e., 73B). CpLDH consists of 321 residues that are numbered from the initiator methionine at residue 17 to the C-terminal residue Ala337. Insertions occur at six places in the sequence, where amino acid designations have a letter appended to the number.

Acknowledgement

This work was supported by a research grant #106493 35 RGGN from amfAR.

Author Contributions

OS was responsible for cloning, expression, purification, enzyme assay, crystallization and intensity data collection. WJC was involved in structure solution, model building and refinement. HS participated in cloning, expression, purification, enzyme assay, crystallization and intensity data collection. AH was responsible for calculation of kinetic parameters. DC was responsible for overall supervision, intensity data collection, data processing, model building and refinement. All authors contributed to manuscript preparation.

References

M.S. Abrahamsen, T.J. Templeton, S. Enomoto, J.E. Abrahante, G. Zhu, C.A. Lancto, M. Deng, C. Liu, G. Widmer, S. Tzipori, G.A. Buck, P. Xu, A.T. Bankier, P.H. Dear, B.A. Konfortov, H.F. Spriggs, L. Iyer, V. Anantharaman, L. Aravind, V. Kapur, Complete genome sequence of the apicomplexan, *Cryptosporidium parvum*, Science 304 (2004) 441-445.

L.K. Basco, F. Marquet, M.M. Makler, J. Le Bras, *Plasmodium falciparum* and *Plasmodium vivax*: lactate dehydrogenase activity and its application for in vitro drug susceptibility assay, Exp. Parasitol. 80 **(**1995) 260-271.

J. I. Boucher, J. R. Jacobowitz, B. C. Beckett, S. Classen, D. L. Theobald, An atomic-resolution view of neofunctionalization in the evolution of apicomplexan lactate dehydrogenases, Elife (2014) e02304

J.C. Bressi, C.L. Verlinde, A.M. Aronov, M.L. Shaw, S.S. Shin, L.N. Nguyen, S. Suresh, F.S. Buckner, W.C. Van Voorhis, I.D. Kuntz, W.G.J. Hol, M.H. Gelb, Adenosine analogues as selective inhibitors of glyceraldehyde-3-phosphate dehydrogenase of *Trypanosomatidae* via structure-based drug design, J. Med. Chem. 44 (2000) 2080-2093.

A. T. Brünger, P. D. Adams, G.M. Clore, W.L. Delano, P. Gross, R.W. Grosse-Kunstleve, J. S. Jiang, J. Kuszewski, M. Nilges, N.S. Pannu, R.J. Read, L.M. Rice, T. Simonson, G.L. Warren, Crystallography and NMR system (CNS): A new software system for macromolecular structure determination, Acta Cryst. D54 (1998) 905-921.

D.J. Bzik, B. A. Fox, K. Gonyer, Expression of Plasmodium falciparum lactate dehydrogenase in *Escherichia coli*. Mol. Biochem. Parasitol. 59 (1993) 155-166.

A. Chaikuad, V. Fairweather, R. Conners, T. Joseph-Horne, D. Turgut-Balik, R.L. Brady, Structure of lactate dehydrogenase from *Plasmodium vivax*: Complexes with NADH and APADH, Biochemistry 44 (2005) 16221-16228.

Collaborative Computational Project, Number 4, Acta Cryst. D50 (1994) 760-763.

R. Conners, F. Schambach, J. Read, A. Cameron, R.B. Sessions, L. Vivas, A., Easton, S.L. Croft, R.L. Brady, Mapping the binding site for gossypol-like inhibitors of *Plasmodium falciparum* lactate dehydrogenase, Mol. Biochem. Parasitol. 142 (2005) 137-148.

G.H. Coombs, Biochemical peculiarities and drug targets in *Cryptosporidium parvum*: lessons from other coccidian parasites, Parasitol. Today 15 (1999) 333-338.

C. Dando, E.R. Schroeder, L.A. Hunsaker, L.M. Deck, R.E. Royer, X. Zhou, S.F. Parmley, D.L. Vander Jagt, The kinetic properties and sensitivities to inhibitors of lactate dehydrogenases (LDH1 and LDH2) from *Toxoplasma gondii*: comparisons with pLDH from *Plasmodium falciparum*, Mol. Biochem. Parasitol. 118 (2001) 23-32.

I.W. Davis, A. Leaver-Fay, V.B. Chen, J.N. Block, G.J. Kapral, X. Wang, L.W. Murray, W.B. Arendall 3rd, J. Snoeyink, J.S. Richardson, D.C. Richardson, MolProbity: all-atom contacts and structure validation for proteins and nucleic acids, Nucleic Acids Res. 35 (2007) W375-W383.

L.M. Deck, R.E. Royer, B.B. Chamblee, V.M. Hernandez, R.R. Malone, J.E. Torres, L.A. Hunsaker, R.C. Piper, M.T. Makler, D.L. Vander Jagt, Selective inhibitors of human lactate dehydrogenases and lactate dehydrogenases from the malarial parasite *Plasmodium falciparum*, J. Med. Chem. 41 (1998) 3879-3887.

W.L. Delano, The PyMOL Molecular Graphics System, (2002) http://www.pymol.org.

S. Dempster, S. Harper, J.E. Moses, I. Dreveny, Structural characterization of the apo form and NADH binary complex of human lactate dehydrogenase, Acta Cryst. D70 (2014) 1484-1490.

H. Denton, S.M. Brown, C.W. Roberts, J. Alexander, V. McDonald, K.W. Thong, G.H. Coombs, Comparison of the phosphofructokinase and pyruvate kinase activities of *Cryptosporidium parvum*, *Eimeria tenella* and *Toxoplasma gondii*, Mol. Biochem. Parisitol. 76 (1996) 23-29.

C.R. Dunn, M.J. Banfield, J.J. Barker, C.W, Higham, K.M. Moreton, D. Turgut-Balik, R.L. Brady, J.J. Holbrook, The structure of lactate dehydrogenase from *Plasmodium falciparum* reveals a new target for anti-malarial design, Nat. Struct. Biol. 3 (1996) 912-915.

P. Emsley, B. Lohkamp, W.G. Scott, K. Cowtan, Features and development of Coot, Acta Cryst. D66 (2010) 486-501.

R.A. Engh, R. Huber, Accurate bond and angle parameters for x-ray protein structure refinement, Acta Cryst. A47 (1991) 392–400.

W. Eventoff, M.G. Rossmann, S.S. Taylor, H.J. Torff, H. Meyer, W. Keil, H.H. Kiltz, Structural adaptations of lactate dehydrogenase isozymes, Proc. Natl. Acad. Sci. USA 74 (1977) 2677-2681.

J. Everse, N.O. Kaplan, Lactate dehydrogenase: structure and function, Adv. Enzymol. Relat. Areas Mol. Biol. 37 (1973) 61-133.

M.S. Gomez, R.C. Piper, L.A. Hunsaker, R.E. Royer, L.M. Deck, M.T. Makler, D.L. Vander Jagt, Substrate and cofactor specificity and selective inhibition of lactate dehydrogenase from the malarial parasite *Plasmodium falciparum*, Mol. Biochem. Parasitol. 90 (1997) 235-246.

P. Gouet, E. Courcelle, D.I. Stuart, F. Metoz, ESPript: multiple sequence alignments in PostScript, Bioinformatics 15 (1999) 305-308.

M. Goujon, H. McWilliam, W. Li, F. Valentin, S. Squizzato, J. Paern, R. Lopez, A new bioinformatics analysis tools framework at EMBL-EBI, Nucleic Acids Res. 38 (2010) W695-699.

A. Hernandez, M.T. Ruiz, An EXCEL template for calculation of enzyme kinetic parameters by non-linear regression. Bioinformatics 14 (1998) 227-228.

K.L. Kavanagh, R.A. Elling, D.K. Wilson, Structure of *Toxoplasma gondii* LDH1: Active-site differences from human lactate dehydrogenases and the structural basis for efficient $APAD^+$ use, Biochemistry 43 (2004) 879-889.

P. Klenerman, H. Dickson, Plasma lactate dehydrogenase estimation in the diagnosis of malaria, Ann. Trop. Med. Parasitol. 86 (1992) 563-565.

G.J. Leitch, Q He, Cryptosporidiosis - an overview, J. Biomed. Res. 25 (2012) 1-16.

D. Madern, X Cai, M.S. Abrahamsen, G. Zhu, Evolution of *Cryptosporidium parvum* lactate dehydrogenase from malate dehydrogenase by a very recent event of gene duplication, Mol. Biol. Evol. 21 (2004) 489-497.

M.T. Makler, D.J. Hinrichs, Measurement of the lactate dehydrogenase activity of *Plasmodium falciparum* as an assessment of parasitemia, Am. J. Trop. Med. Hyg. 48 (1993) 205-210.

G.N. Murshudov, P. Skubák, A.A. Lebedev, N.S. Pannu, R.A. Steiner, R.A. Nicholls, M.D. Winn, F. Long, A.A. Vagin, REFMAC5 for the refinement of macromolecular crystal structures, Acta Cryst. *D*67 (2011) 355-367.

K.L. Olgiati, W.A. Jr Toscano. Kinetics of gossypol inhibition of bovine lactate dehydrogenase X, Biochem. Biophys. Res. Comm. 115 (1983) 180-185

Z. Otwinowski, W. Minor, Processing of X-ray diffraction data collected in oscillation mode, Methods Enzymol. 276 (1997) 307-326.

J.A. Read, V.J. Winter, C.M. Eszes, R.B. Sessions, R.L. Brady, Structural basis for altered activity of M- and H-isozyme forms of human lactate dehydrogenase, Proteins: Struct. Funct. Genet. 43 (2001) 175-185.

R.E. Royer, L.M. Deck, N.M. Campos, L.A. Hunsaker, D.L. Vander Jagt, Biologically active deriviatives of gossypol: synthesis and antimalarial activities of peri-acylated gossylic nitriles, J. Med. Chem. 29 (1998) 1799-1801.

M. Santín, Clinical and subclinical infections with Cryptosporidium in animals, N.Z. Vet. J. 61 (2013) 1-10.

O. Senkovich, H. Speed, A. Grigorian, K. Bradley, C.S. Ramarao, B. Lane, G. Zhu, D. Chattopadhyay, Crystallization of three key glycolytic enzymes of the opportunistic pathogen *Cryptosporidium parvum*, Biochim. Biophys. Acta 1750 (2005) 166-172.

R.B. Sessions, V. Dewar, A.R. Clarke, J. Holbrook, A model of *Plasmodium falciparum* lactate dehydrogenase and its implications for the design of improved antimalarials and the enhanced detection of parasitaemia, Protein Eng. 10 (1997) 301-306.

D.A. Shirley, S.N. Moonah, K.L. Kotloff, Burden of disease from cryptosporidiosis, Curr. Opin. Infect. Dis. 25 (2012) 555-563.

F. Sievers, A. Wilm, D. Dineen, T.J. Gibson, K. Karplus, W. Li, R. Lopez, H. McWilliam, M. Remmert, J. Söding, J.D. Thompson, D.G. Higgins, Fast, scalable generation of high-quality protein multiple sequence alignments using Clustal Omega, Mol. Syst. Biol. 7 (2011) 539.

M. Vedadi, J. Lew, J. Artz, M. Amani, Y. Zhao, A. Dong, G.A. Wasney, M. Gao, T. Hills, S. Brokx, W. Qiu, S. Sharma, A. Diassiti, Z. Alam, M. Melone, A. Mulichak, A. Wernimont, J. Bray, P. Loppnau, O. Plotnikova, K. Newberry, E. Sundararajan, S. Houston, J. Walker, W. Tempel, A. Bochkarev, I. Kozieradzki, A. Edwards, C. Arrowsmith, D. Roos, K. Kain, R. Hui, Genome-scale protein expression and structural biology of *Plasmodium falciparum* and related Apicomplexan organisms, Mol. Biochem. Parasitol. 151 (2007) 100-110.

A.D. Waldman, K. W. Hart, A. R. Clarke, D. B. Wigley, D. A. Barstow, T. Atkinson, W. N. Chia, J. J. Holbrook, The use of genetically engineered tryptophan to identify the

movement of a domain of *B. stearothermophilus* lactate dehydrogenase with the process which limits the steady-state turnover of the enzyme, Biochem. Biophys. Res. Commun. 150 (1988) 752-759.

C.C. Wang, Parasite enzymes as potential targets for antiparasitic chemotherapy, J. Med. Chem. 27 (1984) 1-9.

C.S. Wang, Inhibition of human erythrocyte lactate dehydrogenase by high concentration of pyruvate. Evidence for the competitive substrate inhibition. Eur. J. Biochem. 78 (1977), 569-574.

H.M. Wilks, K. W. Hart, R. Feeney, C. R. Dunn, H. Muirhead, W. N. Chia, D. A. Barstow, T. Atkinson, A. R. Clarke, J. J. Holbrook, A specific, highly active malate dehydrogenase by redesign of a lactate dehydrogenase framework. Science 242 (1988) 1541-1544.

V.J. Winter, A. Cameron, R. Tranter, R.B. Sessions, R.L. Brady, Crystal structure of *Plasmodium berghei* lactate dehydrogenase indicates the unique structural differences of these enzymes are shared across the *Plasmodium* genus, Mol. Biochem. Parasitol. 131 (2003) 1-10.

G. Zhu, J. S. Keithly, Alpha-proteobacterial relationship of apicomplexan lactate and malate dehydrogenases. J. Eukaryot. Microbiol. 49 (2002) 255-261.

Figure legends

Figure 1. Sequence alignment

Primary sequences of LDH from various organisms were aligned based on structural homology. The labelling of secondary structural elements corresponds to the CpLDH structure. The three black triangles indicate changes in the CpLDH sequence compared to the GenBank sequence. This figure was prepared using ESPript (Gouet *et al*., 1999).

Figure 2. Enzymatic activity

A. CpLDH activity for reduction of pyruvate was measured using buffer solutions at different pH. Relative activity is plotted against pH values.

B. CpLDH activity for oxidation of lactate was measured using buffer solutions at different pH. Relative activity is plotted against pH values.

C. Ki values for gossypol were determined for reduction of pyruvate with NADH at pH 5.5. Pyruvate concentration was 5 mM, and NADH concentrations were varied between 5-35 μM. Gossypol concentrations were 0, 2.5, 7.5 and 10 μM.

D. *Cp*LDH activity was determined at saturating concentration of NADH (150 μM) and varying concentrations of pyruvate by measuring the decrease in absorbance at 340 nm.

Figure 3. Assembly of CpLDH and details of the cofactor binding pocket

A. Cartoon drawing showing assembly of CpLDH in the asymmetric unit of the ternary complex with NAD^+ and pyruvate. The two monomers comprising the asymmetric unit are related by a noncrystallographic 2-fold axis that is approximately perpendicular to the page. Catalytic and NAD-binding domains of monomer A are depicted in magenta and light pink, respectively. The helix connecting the two domains is shown in red and marine blue in the two subunits. Catalytic and NAD-binding domains of the B subunit are colored cyan and light cyan, respectively, and the connecting helix is shown in slate. NAD^+ and pyruvate are shown as stick models.

B. Close-up view of the NAD binding site in CpLDH, colored as in Figure 3(A). NAD is shown as a stick model (carbon: white). CpLDH residues in the NAD-binding site are also shown as stick models (carbon: rose or magenta).

C. Surface drawing showing a close-up view of the adenine binding pocket in CpLDH. NAD is shown as a stick model (carbon: green). CpLDH residues lining the pocket are shown as stick models (carbon: white) in the semi-transparent surface diagram.

D. Stereoscopic view of the NAD-binding site in the CpLDH/NAD^+/pyruvate complex. NAD (carbon: green), pyruvate (carbon: yellow) and the CpLDH residues (carbon: rose) forming hydrogen bonds to NAD and pyruvate are shown. Arg171 and His195 are also shown in stick model (carbon: magenta). Potential hydrogen bonds are illustrated in dotted lines. Two water molecules near NAD are shown as red spheres.

Figure 4. Changes in CpLDH structure upon substrate and cofactor binding

A. Cartoon drawing showing superposition of the structures of apo CpLDH (magenta) and the ternary complex (cyan) with NAD^+/pyruvate, highlighting the areas that show major changes. These areas are shown in blue on the complex structure, and the amino acid residues are labeled. The active site loop observed in the complex (residues 99-111, colored deep blue) is disordered in the apo-form. NAD (carbon: green) and pyruvate (carbon: yellow) are shown as stick models.

B. Close-up view of the region encompassing residues 138-145 of CpLDH in the apo and ternary complex structures. Amino acid residues are shown as stick models: apo (carbon: rose) and complex (carbon: cyan).

C. Close-up view of the region encompassing residues 194-198 of CpLDH in the apo and ternary complex structures. Amino acid residues are shown as stick models: apo (carbon: rose) and complex (carbon: cyan). The His195 side chain is oriented towards the substrate in the complex.

D. Close-up view of the region encompassing residues 234-245 of CpLDH in the apo and ternary complex structures. Amino acid residues are shown as stick models: apo (carbon: rose) and complex (carbon: cyan). In the complex Trp236 moves closer to the substrate.

Figure 5. Comparison of CpLDH with human LDH.

A. Superposition of A monomers of the ternary complex CpLDH/NAD^+/oxamate (cyan) and human LDH with NADH and oxamate (magenta) (*1I0Z*; Read *et al*., 2001). NAD^+ in CpLDH is shown as a stick model (carbon: green), and oxamate is shown as a ball

and stick model (carbon: yellow). Three loop regions that show significant differences in conformation are labeled on the CpLDH cartoon.

B. Detailed view of the loops covering the entrance to the active site. The labelled residues are from CpLDH. (2Fo-Fc electron density contoured at 1.2σ for the residues in the two loops near the active site is displayed in supplementary figure).

C. Detailed view of the antigenic loops in CpLDH (stick model) and human LDH (red). (2Fo-Fc electron density contoured at 1.2σ for the loop residues in CpLDH is shown in supplementary figure).

Figure 6. Comparison of CpLDH structure with PfLDH and TgLDH

A. Cartoon diagram showing superposition of CpLDH structure (cyan) with PfLDH (yellow) and TgLDH (white) structures. Structures of the CpLDH NAD+/pyruvate complex (*4ND1*), TgLDH/APAD/oxalate complex (*1PZF*) and PfLDH/NAD/oxalate complex (1T2D) were used for superposition. NAD and pyruvate molecules in CpLDH are shown as stick models.

B. A close up view showing the differences in the conformation near the active site of CpLDH. Residues 101-102 that are different in CpLDH as compared to other apicomplexan LDHs are shown as stick models. The conformation of the loop comprising residues 243-246 is also different in CpLDH.

Figure 7. Comparison of CpLDH, PfLDH and TgLDH with CpMDH

A. Superposition of one monomer of CpLDH (*4ND1*, cyan) and CpMDH (*2HJR*, yellow) Only the active site region is shown because the differences are restricted to this area. Substrate binding residues of CpLDH and corresponding residues of CpMDH are shown as stick models (carbon atoms are colored same as the respective protein chain). CpLDH numbering is used for labeling except residue Arg94 of CpMDH, which is shown hydrogen bonded to citrate in the active site of CpMDH.

B. Differences in the active site regions of CpLDH (blue), PfLDH (magenta) and TgLDH (grey) compared to CpMDH (yellow). Glutamine 102 serves as the specificity residue for canonical LDHs. In all MDHs the corresponding residue is an arginine (Arg94 in CpMDH). In apicomplexan LDHs, residue 102 is lysine (Lys102 in TgLDH). In PfLDH and TgLDH there is a five residue insertion in the active site loop. Due to the insertion, residue Trp107 becomes the specificity residue in PfLDH and CpLDH.

However, LDHs of Cryptosporidium are exceptional among apicomplexan LDHs in that residue 102 in CpLDH is glycine. Residue 103 is an arginine in CpLDH, and it remains excluded from the active site.

Figure 8. Hydrogen bonding interactions in the active site of LDH

A. Human LDH NAD^+/oxamate complex (1I0Z, Read *et al*., 2001) Stick diagram showing amino acid residues and water molecules forming hydrogen bonds with NAD and oxamate.

B. CpLDH NAD+/oxamate complex (*4ND1*). Amino acid residues involved in hydrogen bonding interactions with NAD and oxamate.

Figure 9. Comparison of NAD^+ and $APAD^+$ binding in CpLDH. The $APAD^+$ carbon atoms are light green; the NAD+ carbons are light magenta. Important residues in the active site are included as stick models.

Table 1. Comparison of kinetic parameters for CpLDH, TgLDHs, PfLDH and human LDHs

	CpLDH				PfLDH		Hs_M		Hs_H		TgLDH1		TgLDH2	
	K_m	K_{cat}	K_{cat}/K_m	*h*	K_m	K_{cat}	K_m	K_{cat}	K_m	K_{cat}	K_m	K_{cat}	K_m	K_{cat}
Pyruvte	197.3±0.1	124.0±5.6	0.63±0.04	0.69±0.00	30	27	170	18	55	13	120	35	800	4.6
Lactat*	1.8±0.2	2.7±0.3	0.002±0.141	N.D.	12.0	17	11.0	4.9	13.0	3	8.0	1.6	54.0	5.8
NADH	16.9±0.0	125.2±3.9	7.41±0.03	1.23±0.03	7	27	5	18	8	13	4.2	37	1.9	4.3
APAH	16.6±0.0	231.7±7.2	13.96±0.03	1.08±0.06										
NAD^+	30.3±0.0	3.3±0.1	0.11±0.03	1.04±0.07	86	17	93	4.9	37	3	348	1.3	640	0.45
$APAD^+$	8.5±0.1	14.9±0.8	1.75±0.05	0.69±0.08	123	51	56	0.24	37	0.17	50	34	78	13

Units: K_m in μM, except for lactate* (mM); K_{cat} in $min^{-1} \times 10^{-3}$; K_{cat}/K_m in $M^{-1}\ min^{-1} \times 10^{-3}$.

K_m: Concentration of substrate at which the catalytic rate is half-maximal; K_{cat}: number of substrate molecules processed per molecule of enzyme per unit of time. K_{cat}/K_m: specifity constant; *h* :Hill coefficient (cooperativity); N.D.: not determined.

Data for TgLDH taken from Dano *et al*., 2001; for PfLDH and human LDHs (Hs_H and Hs_M) are taken from Gomez *et al*., 1997.

Hs_H and Hs_M refer to the H and M isoforms.

Table 2

Table 2. Data-collection statistics

	Apoenzyme	NAD^+ , pyruvate	NADH, lactate	NAD^+, oxamate	$APAD^+$, pyruvate
PDB ID	4ND5	4ND4	4ND3	4ND1	4ND2
Crystal data					
Space group	$P3_212$	$P3_221$	$P3_221$	$P3_221$	$P3_221$
Unit cell parameters (Å)	a =b= 136.5	a =b= 95.9	a =b= 95.5	a =b= 94.816	a =b= 95.8
	c= 170.2	c = 185.7	c = 186.0	c - 185.072	c = 185.6
Vm ($Å^3$ Da^{-1})	3.38	3.43	3.61	3.56	3.66
Solvent content (%)	63.6	64.1	65.9	65.5	66.4
Resolution range (Å)	20.0-2.10 (2.17-2.10)†	50.0-2.20 (2.24-2.20)	50.0-2.30 (2.34-2.30)	50.0-2.15 (2.23-2.15)	50.0-2.00 (2.07-2.00)
Overall I/σ	9.2	7.7	9.0	6.7	9.5
No. of unique reflections	100,051	51,036	44194	53149	67,287
Multiplicity	3.8 (3.1)	7.3 (7.0)	8.7 (8.8)	6.7 (4.3)	10.7 (8.7)
Completeness (%)	94.9 (64.6)	99.8 (100.0)	100.0 (99.5)	95.1 (65.7)	99.8 (97.7)
R_{merge}	0.062 (0.290)	0.081 (0.316)	0.064 (0.278)	0.074 (0.041)	0.054 (0.186)

†Values in parentheses refer to the outermost resolution shell.

Table 3

Table 3. Refinement statistics

	Apoenzyme	NAD^+ , pyruvate	NADH, lactate	NAD^+, oxamate	$APAD^+$, pyruvate
PDB ID	4ND5	4ND4	4ND3	4ND1	4ND2
Resolution range (Å)	19.88-2.10 (2.154-2.10)†	49.64-2.20 (2.257-2.20)	40.35-2.05 (2.102-2.049)	47.41-2.15 (2.21-2.15)	49.61-2.00 (2.052-2.00)
Reflections (working set)	91,538 (3950)	45,828 (3316)	55,896 (4102)	45,370 (2221)	60,473 (4312)
Reflections (test set)	4880 (191)	5134 (378)	6253 (441)	5088 (233)	6816 (476)
R value	0.232 (0.292)	0.203 (0.245)	0.220 (0.315)	0.208 (0.291)	0.193 (0.218)
Free R value	0.255 (0.326)	0.223 (0.283)	0.241 (0.309)	0.236 (0.319)	0.208 (0.248)
No. of protein atoms	8909	4710	4710	4710	4710
No. of hetero atoms	0	130	112	124	118
No. of water molecules	194	260	206	150	416
Total no. of glycerol	0	5 [3+2]*	3 [2+1]	4 [3+1]	3 [2+1]
Estimated coordinate error					
based on R value (Å)	0.206	0.205	0.174	0.209	0.145
based on free R value (Å)	0.177	0.169	0.153	0.177	0.127
R.m.s. deviations from ideal values					
Bond lengths (Å)	0.004	0.004	0.005	0.004	0.005
Bond angles (°)	0.844	0.960	0.952	0.954	0.895
Average B value§					
All atoms ($Å^2$)	52.5	36.3	43.3	48.5	27.3
Protein	50.4, 44.0, 53.6, 67.6	33.0, 40.3	39.1, 48.5	45.9, 52.1	25.1, 29.2
Cofactor	-	26.7, 35.3	31.8, 40.9	38.6, 47.7	19.4, 25.2
Substrate/analog		30.6, 37.1	36.3-	39.4, 44.2	20.4, 24.6
Glycerol		55.6, 53.4	55.7, 63.9	62.1, 59.4	37.6, 36.5
Water	44.1	38.7	43.2	46.5	36.1
Structure quality					
Clashscore (percentile)	3.06 (99)	1.24 (100)	1.34 (100)	1.34 (100)	1.55 (100)
MolProbity score (percentile)	1.36 (99)	1.04 (100)	0.99 (100)	1.06 (100)	0.95 (100)
Ramachandran favored (%)	96.12	96.83	97.30	96.83	97.78
Ramachandran allowed (%)	3.63	2.54	2.22	2.69	2.06
Ramachandran outliers (%)	0.25	0.63	0.48	0.48	0.16

Rotamer outliers (%)	0.31	0.19	0.39	0.00	0.19

† numbers in parenthesis are for highest resolution shell

*number of glycerol molecule associated with each monomer in the asymmetric unit.

§values for different subunits in asymmetric unit are separated by comma

Figure 1

Click here to download high resolution image

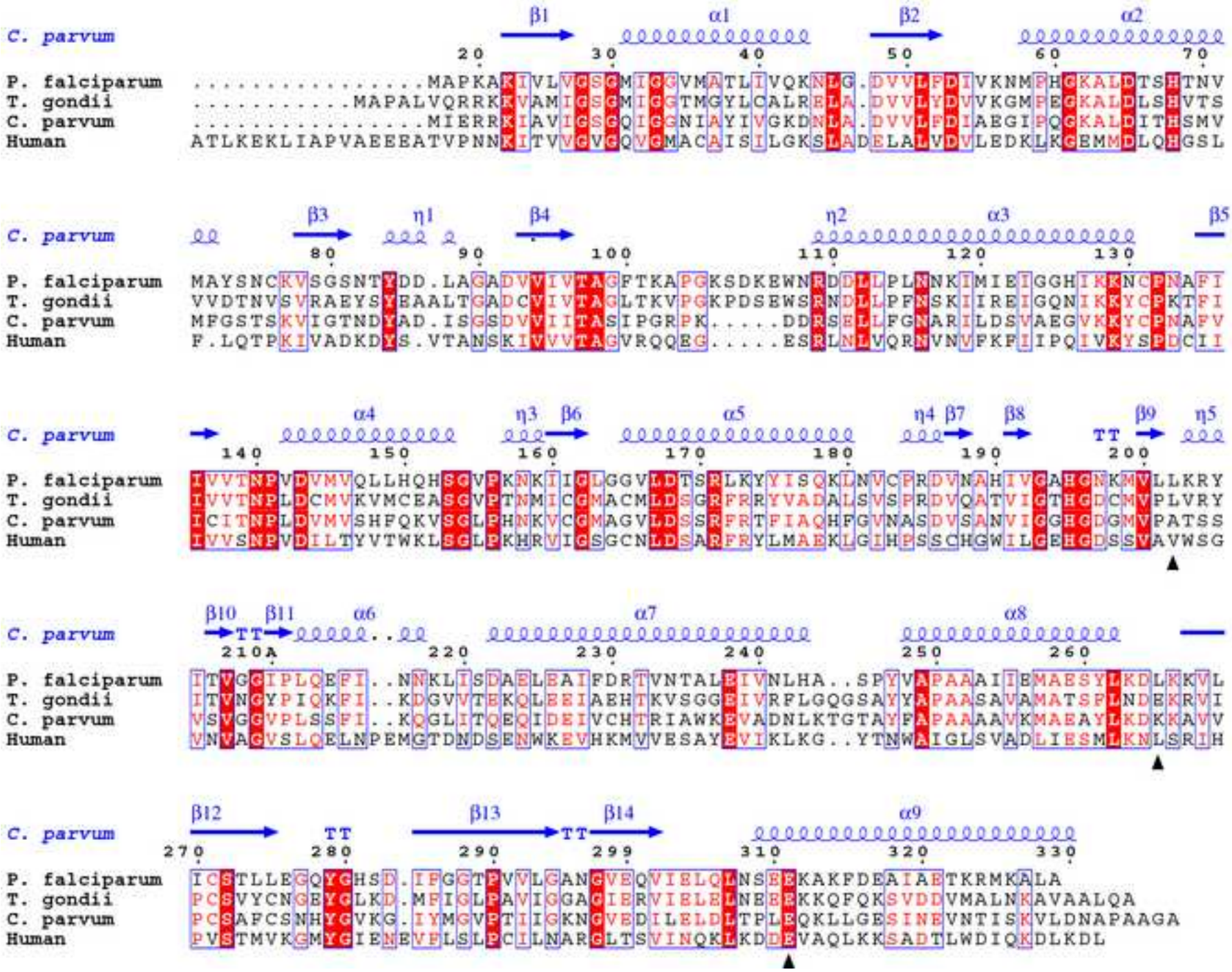

Figure 2

A

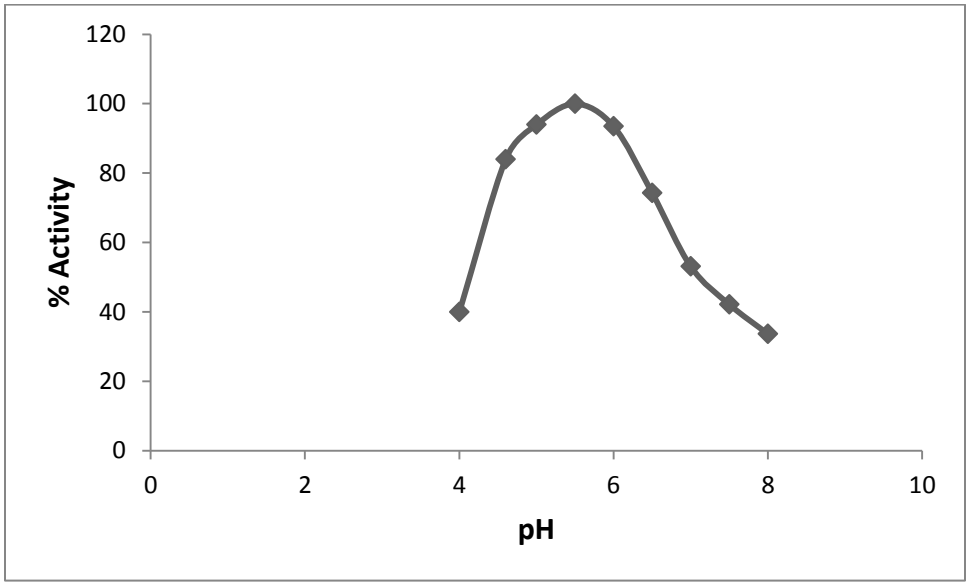
120
100
80
60
40
20
0
% Activity
0
2
4
6
8
10
pH

B

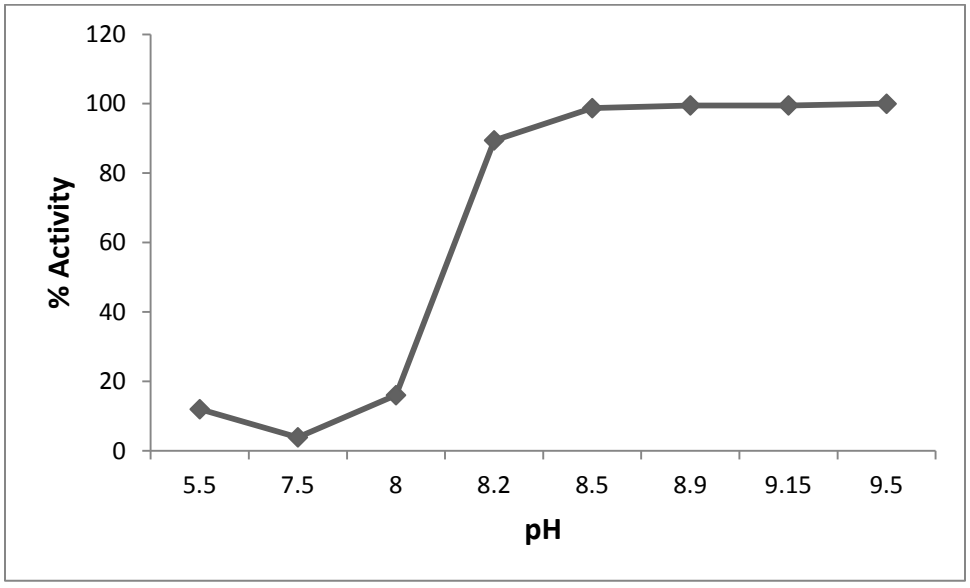
120
100
80
60
40
20
0
% Activity
5.5
7.5
8
8.2
8.5
8.9
9.15
9.5
pH

C

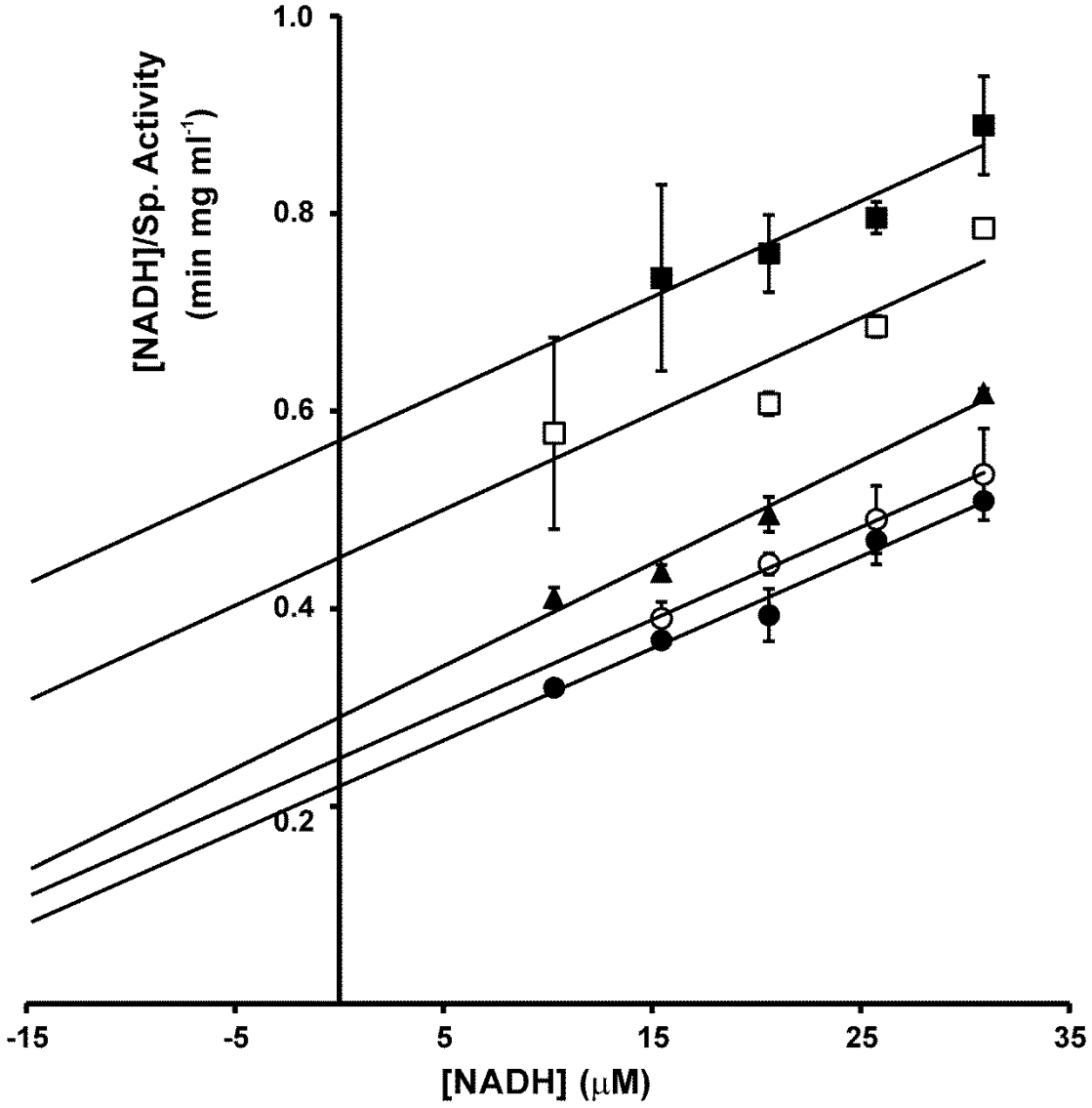

K_m= 26.5±0.1 μM
K_{cat} (10^{-3})= 38.2±1.1 min^{-1}
K_i= 11.6±0.3 μM

● [I]=0 μM
○ [I]=2.5 μM
▲ [I]=5.0 μM
□ [I]=7.5 μM
■ [I]=10.0 μM

D

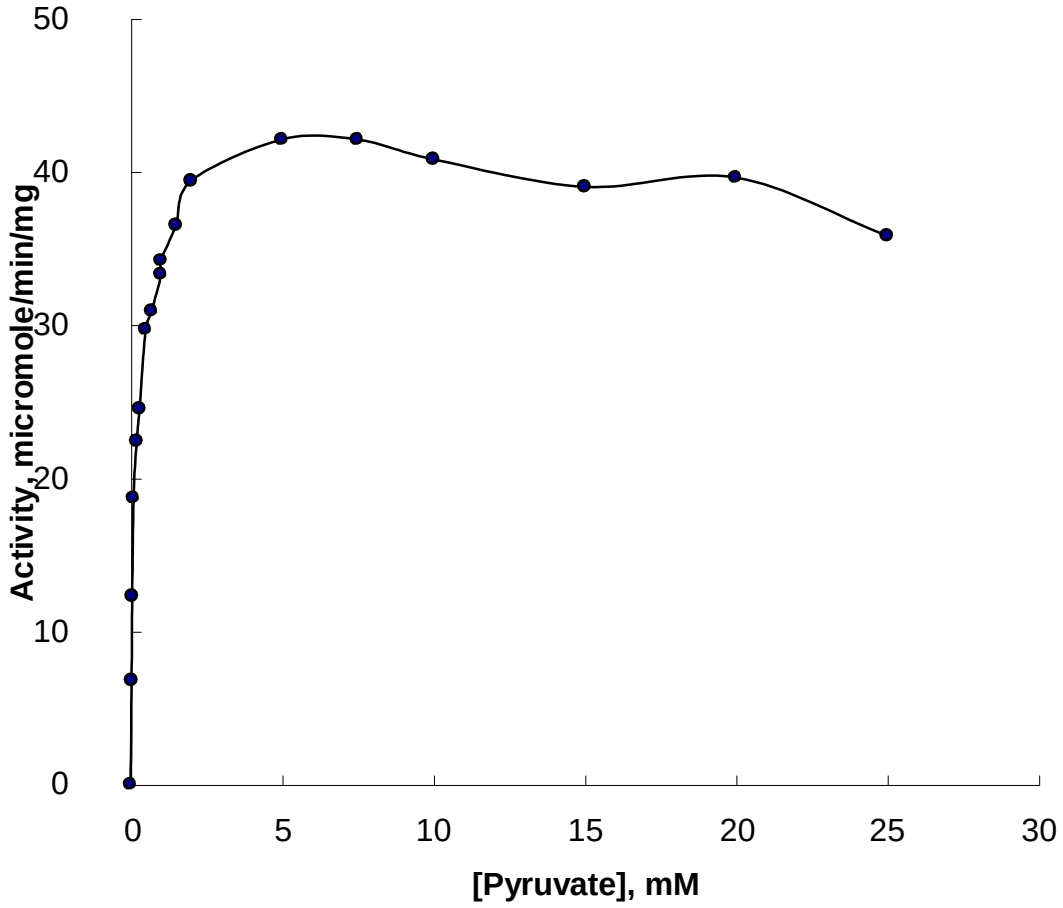
50
40
30
20
10
0
Activity, micromole/min/mg
0
5
10
15
20
25
30
[Pyruvate], mM

Figure 3

Click here to download high resolution image

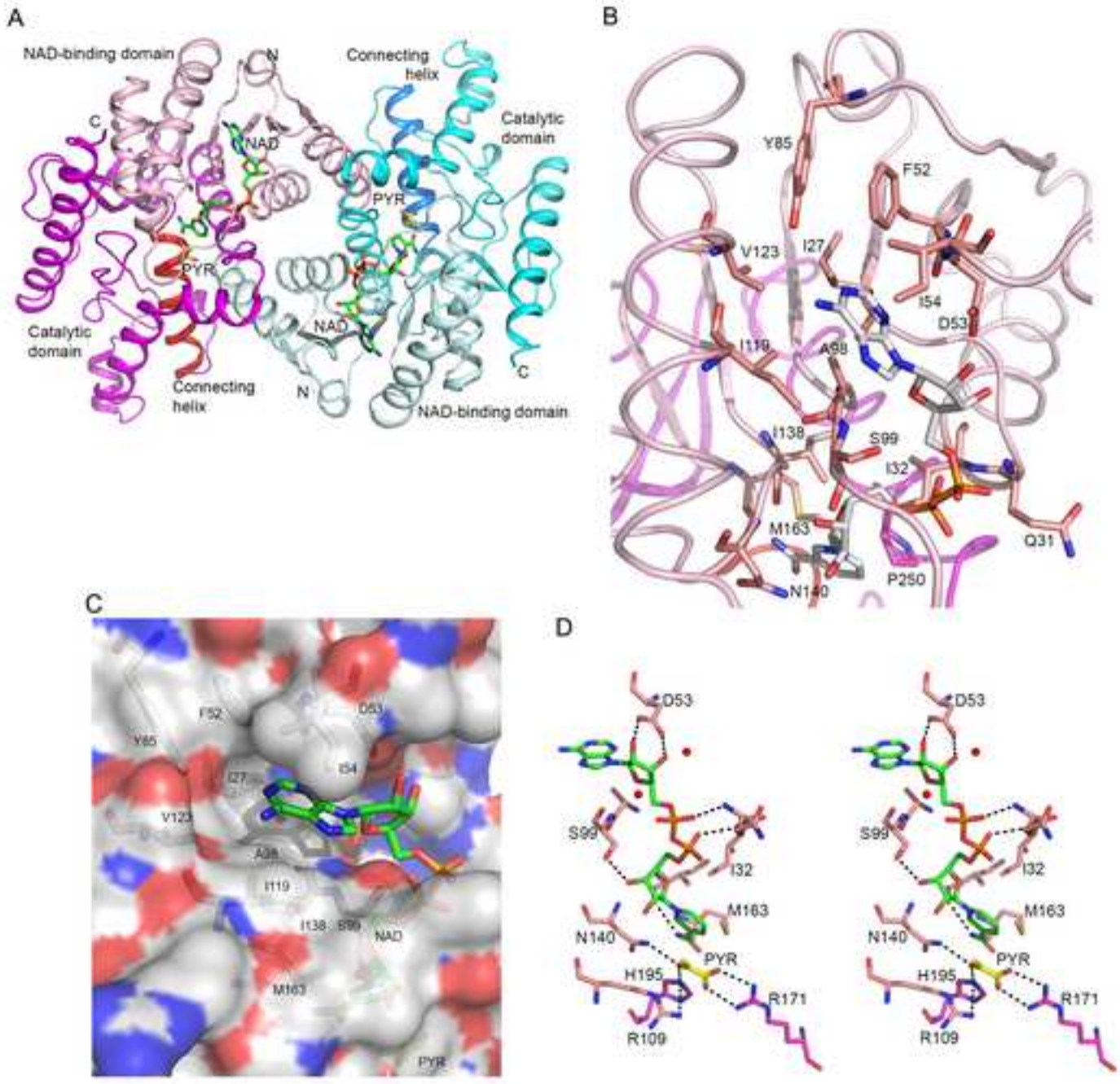

Figure 4

Click here to download high resolution image

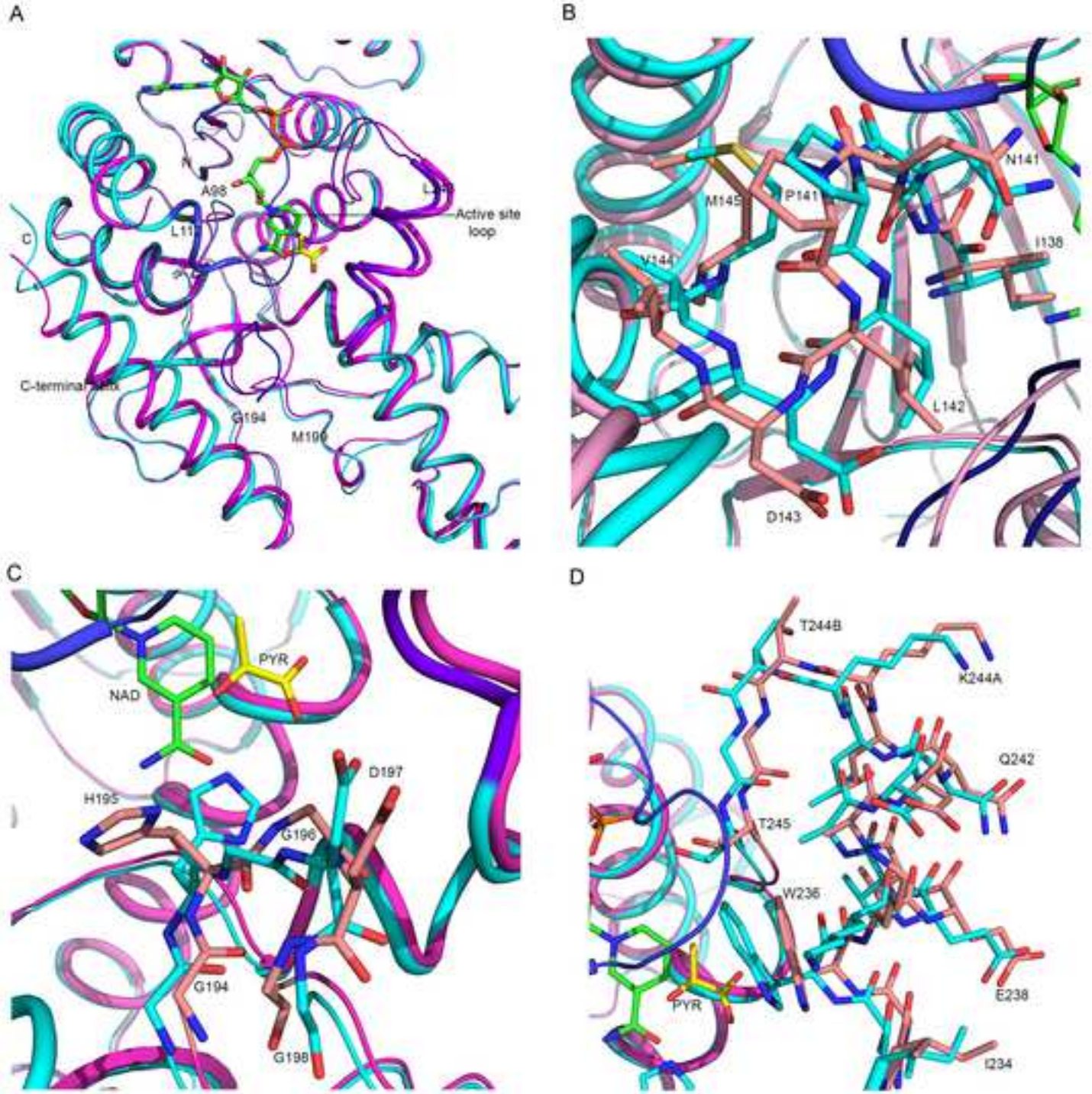

Figure(s)

Click here to download high resolution image

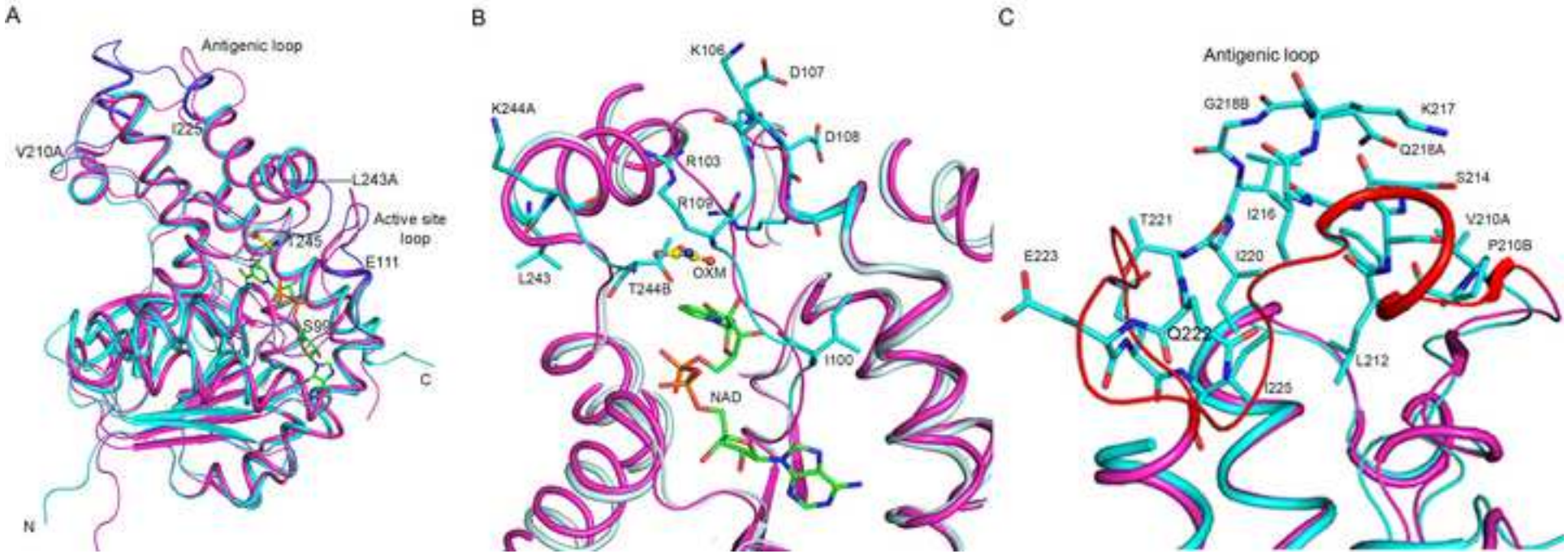

Figure 6

Click here to download high resolution image

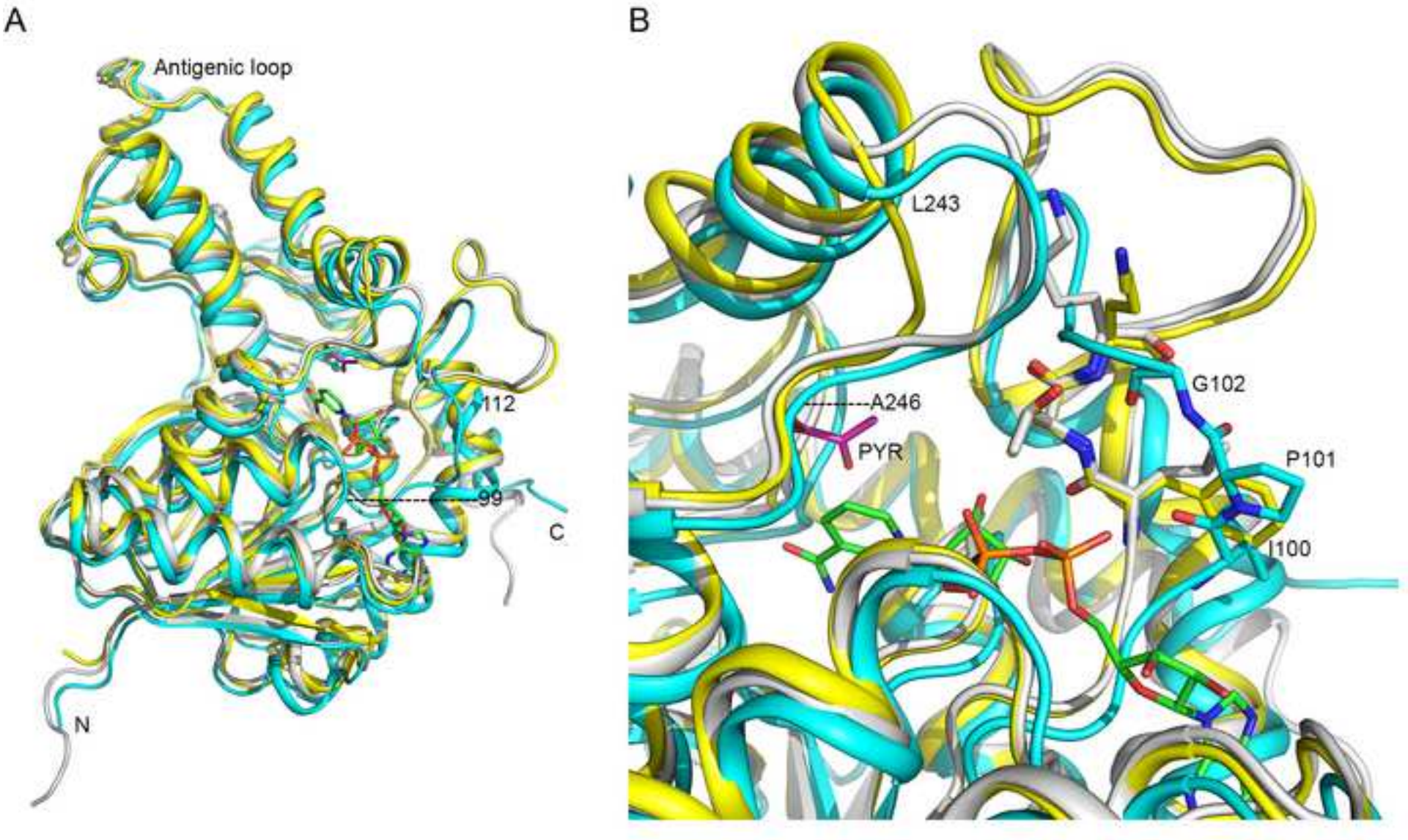

Figure 7

Click here to download high resolution image

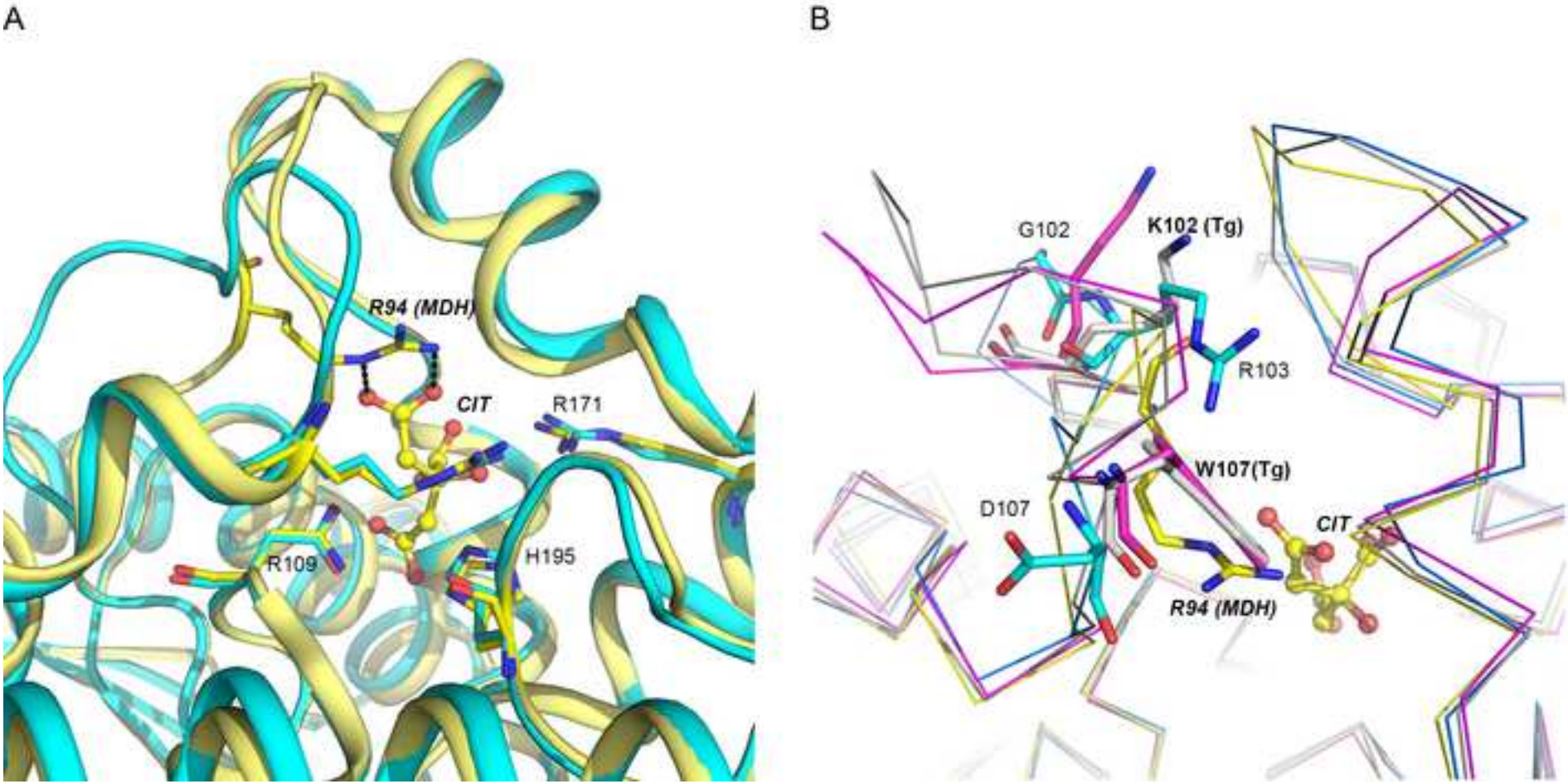

Figure 8

Click here to download high resolution image

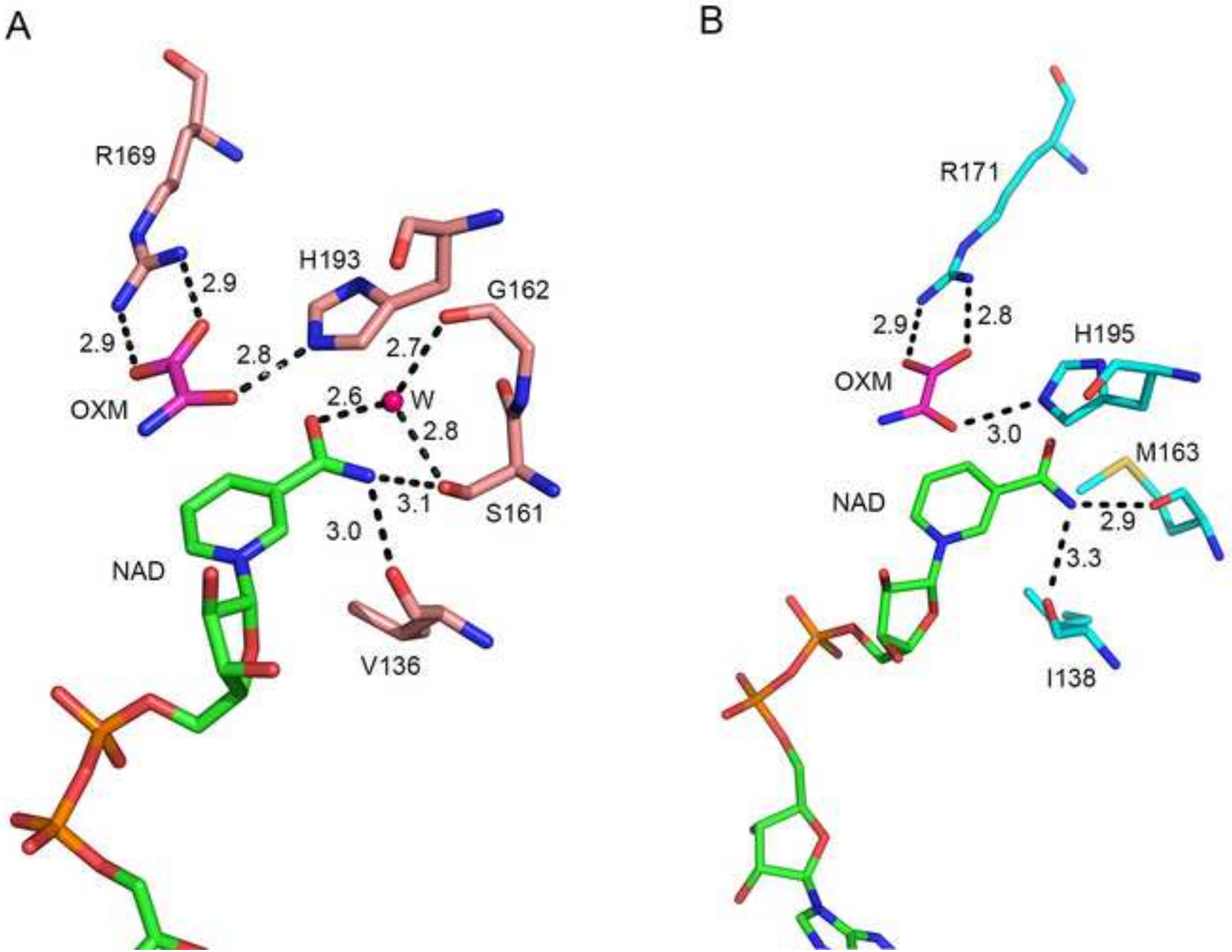

Figure 9

Click here to download high resolution image

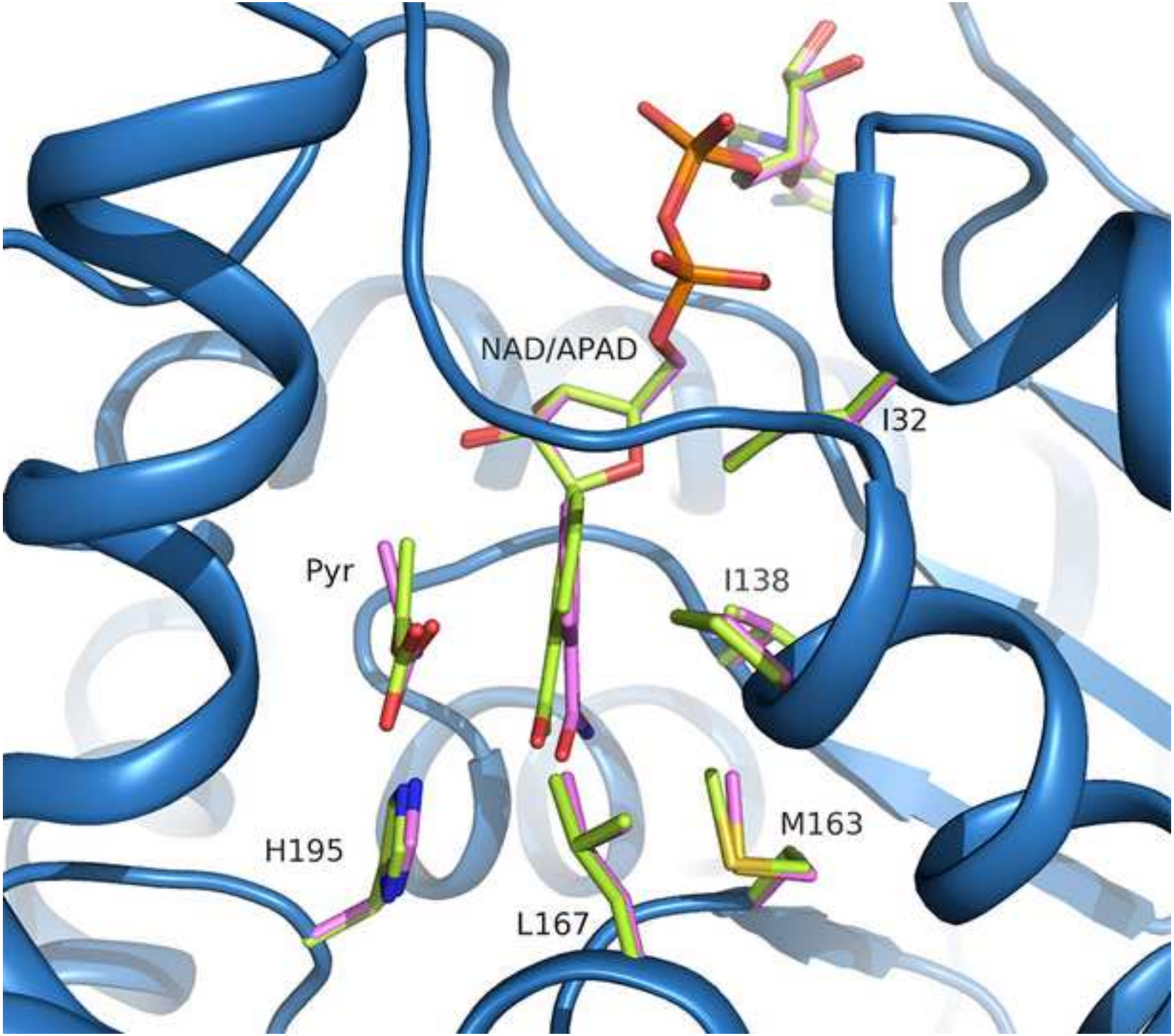

Enzymatic characterization and crystallographic analysis *Cryptosporidium parvum* Lactate dehydrogenase reveal distinctive features of the parasitic enzyme and suggest that it is an exceptional member in the apicomplexan lactate dehydrogenase family.

Supplementary Figure S2

Electron density for substrate and cofactor in the four ternary complexes. For A-D, Fo-Fc electron density maps were generated after removal of ligands. Electron density contoured at 3σ is displayed around each ligand.
(A) CpLDH/NAD^+/pyruvate (4ND4).
(B) CpLDH/NADH/lactate (4ND3).
(C) CpLDH/NAD^+/oxamate (4ND1).
(D) CpLDH/$APAD^+$/pyruvate (4ND2).

For E and F, stereo diagrams showing 2Fo-Fc electron density map are contoured at 1.2σ around ligands, amino acid residues and selected water molecules. (E) CpLDH/NADH/lactate (4ND3).
(F) CpLDH/NAD/oxamate (4ND1).

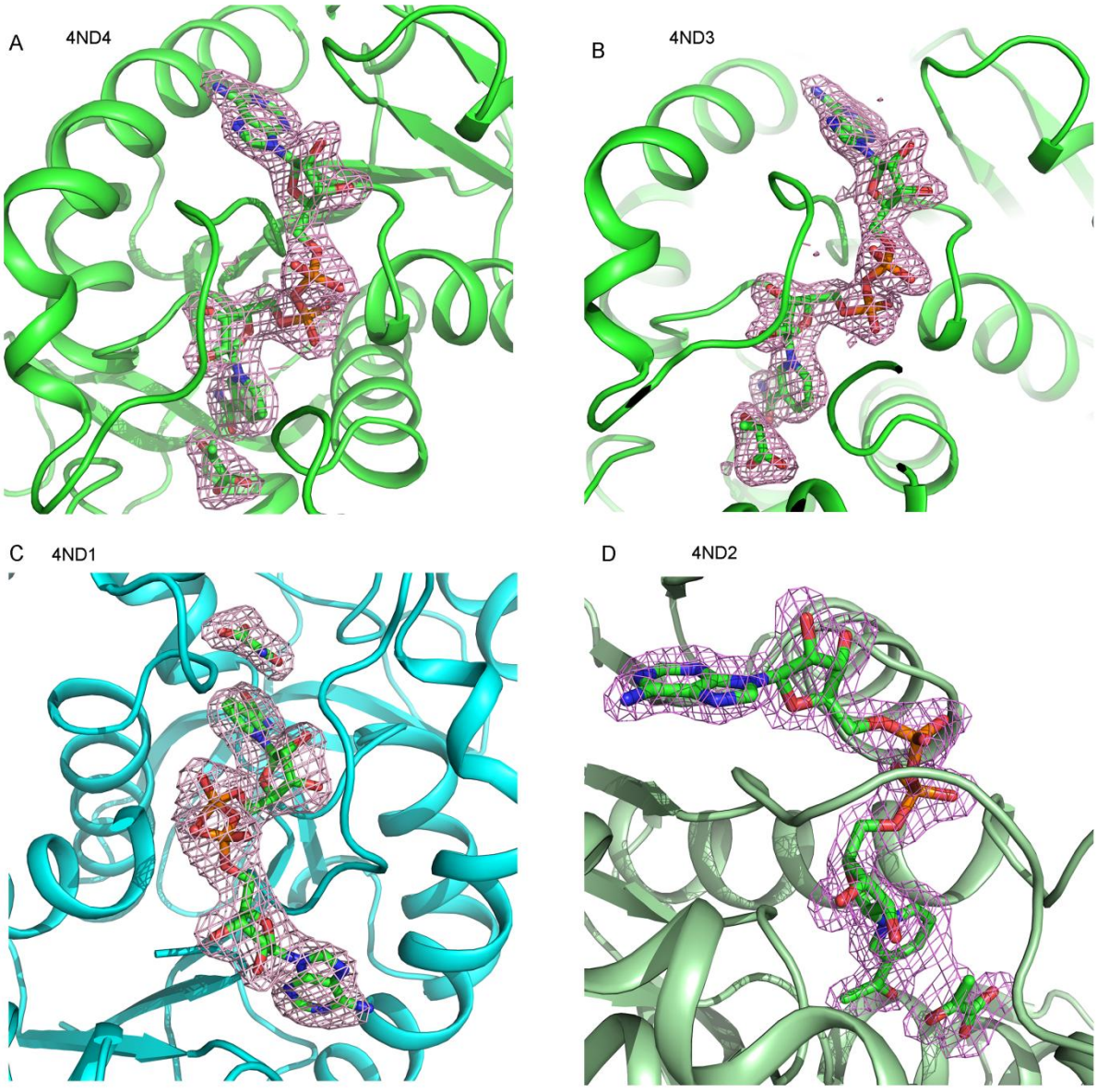
A
4ND4
B
4ND3
C
4ND1
D
4ND2

E 4ND3

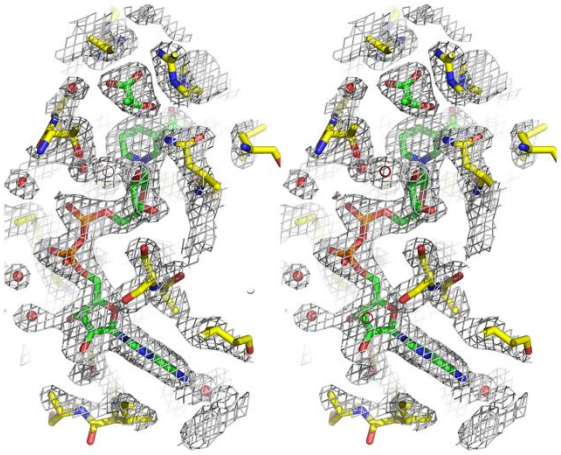

F 4ND1

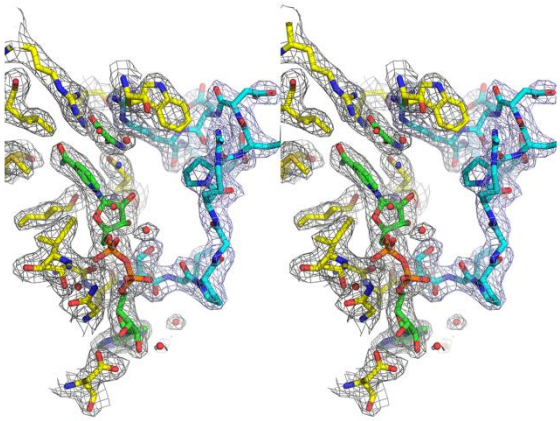

Supplementary Figure S2
Click here to download high resolution image

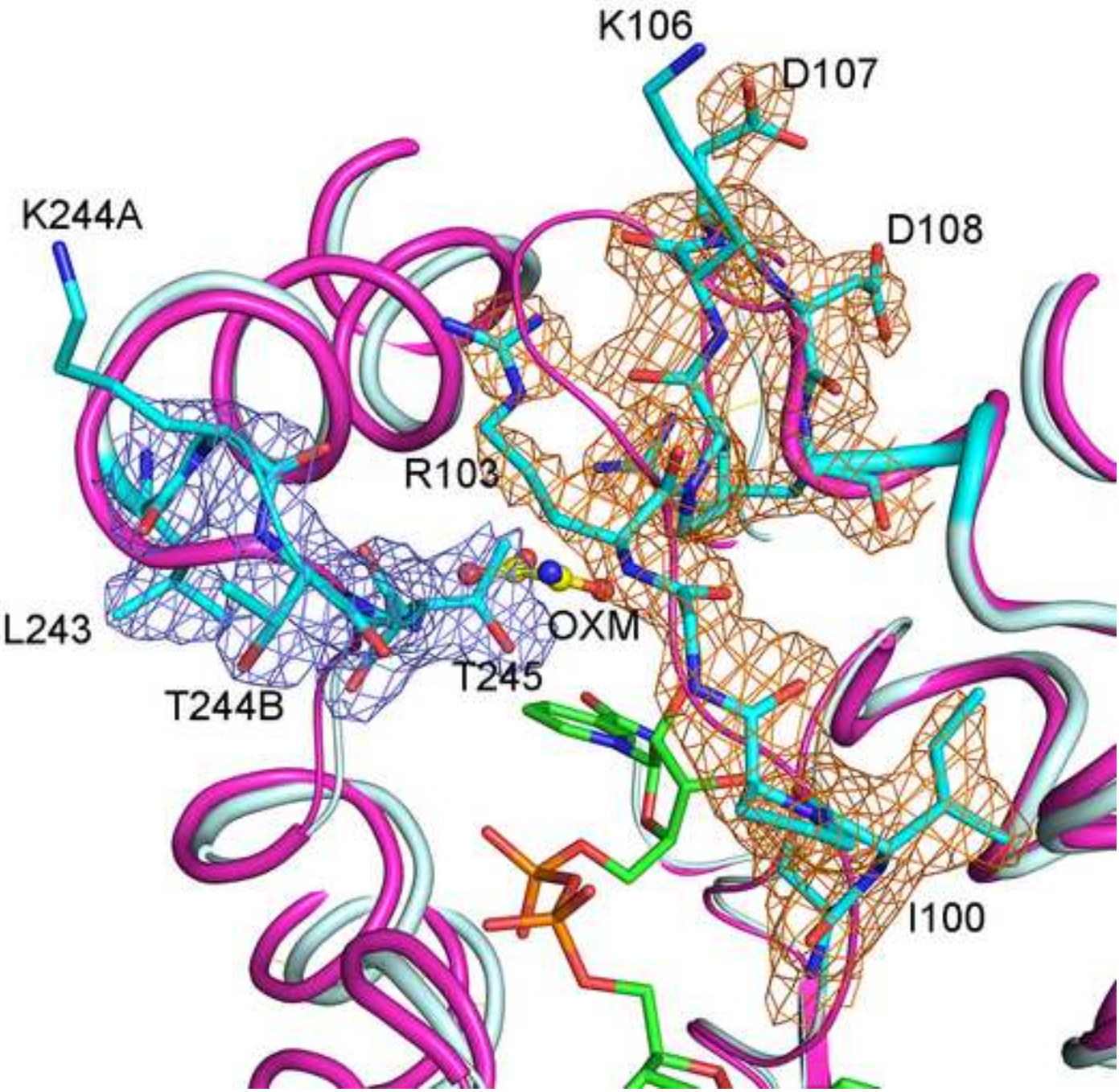

Supplementary Figure S3

Click here to download high resolution image